Statistical Analysis of the Nonlinear Response of Bladed Disks with Mistuning and Cracks

Meng-Hsuan Tien,* Tianyi Hu,† and Kiran D'Souza‡
The Ohio State University, Columbus, Ohio 43210

DOI: 10.2514/1.J058190

In this paper, efficient techniques are presented for analyzing the dynamics of mistuned bladed disks with cracks. The analysis of the influence of cracks, coupled with the influence of mistuning on the dynamics of bladed disks, is computationally challenging for several reasons: 1) complex geometry of modern turbines results in very high-dimensional computational models; 2) mistuning in these structures breaks the cyclic symmetry in these systems; and 3) cracks further disrupt the symmetry and introduce a piecewise-linear nonlinearity into these systems. Recently, several approaches have been developed to handle these challenges individually. The component mode mistuning approach was developed to efficiently model small mistuning in bladed disks. The X-X_r method was developed for generating reduced-order models of cyclically symmetric systems with cracks. More recently, the generalized bilinear amplitude approximation technique was created to efficiently approximate the nonlinear vibrational response of a class of piecewise-linear nonlinear systems. This paper modifies and combines these techniques, for the first time, to enable efficient modeling and statistical analysis of bladed disks with mistuning and cracks. The novel method is able to generate the reduced-order model of full-bladed disks using only single-sector models and approximate the nonlinear vibrational response of the system with significantly reduced computational effort. A high-dimensional finite element model of a mistuned bladed disk with a crack is studied using the proposed approach. The influence of mistuning patterns and cracks on the vibrational response of the bladed disk is discussed.

Nomenclature

$\boldsymbol{C}_{\mathrm{ROM},s}$, $\boldsymbol{C}_{\mathrm{ROM},o}$	=	damping matrices in reduced coordinates
$\boldsymbol{C}_s$, $\boldsymbol{C}_o$	=	damping matrices in global coordinates
$\bar{\boldsymbol{C}}_s$, $\bar{\boldsymbol{C}}_o$	=	damping matrices in relative coordinates
E_i	=	Young's modulus of ith blade
E_0	=	Young's modulus for tuned system
$\boldsymbol{F}$	=	forcing vector in global coordinates
$\boldsymbol{F}_{\mathrm{ROM},s}$, $\boldsymbol{F}_{\mathrm{ROM},o}$	=	forcing vectors in reduced coordinates
$\bar{\boldsymbol{F}}$	=	forcing vector in relative coordinates
$f_{s,j}$, $f_{o,k}$	=	modal forces
$\boldsymbol{I}$	=	identity matrix
$\boldsymbol{K}_{\mathrm{ROM},s}$, $\boldsymbol{K}_{\mathrm{ROM},o}$	=	stiffness matrices of tuned system in reduced coordinates
$\boldsymbol{K}^m_{\mathrm{ROM},s}$, $\boldsymbol{K}^m_{\mathrm{ROM},o}$	=	stiffness matrices of mistuned system in reduced coordinates
$\boldsymbol{K}_s$, $\boldsymbol{K}_o$	=	stiffness matrices in global coordinates
$\bar{\boldsymbol{K}}_s$, $\bar{\boldsymbol{K}}_o$	=	stiffness matrices in relative coordinates
$\boldsymbol{M}_{\mathrm{ROM},s}$, $\boldsymbol{M}_{\mathrm{ROM},o}$	=	mass matrices in reduced coordinates
$\boldsymbol{M}_s$, $\boldsymbol{M}_o$	=	mass matrices in global coordinates
$\bar{\boldsymbol{M}}_s$, $\bar{\boldsymbol{M}}_o$	=	mass matrices in relative coordinates
N	=	number of sectors
N_s, N_o	=	numbers of modes in modal projections
$\boldsymbol{p}_i^b$	=	modal participation factors of ith blade
$\boldsymbol{q}_s$, $\boldsymbol{q}_o$, $q_{s,j}$, $q_{o,k}$	=	modal coordinates
$s_{1,j}$, $s_{2,j}$, $o_{1,k}$, $o_{2,k}$	=	scalar coefficients in transient responses
T_s, T_o	=	time the system spends in sliding and open states
$\boldsymbol{T}_v$	=	projection matrix
$\boldsymbol{u}_s$, $\boldsymbol{u}_o$	=	reduced coordinates
$\bar{\boldsymbol{u}}_o$	=	open system reduced space projection onto sliding system reduced space
$\dot{\hat{\boldsymbol{u}}}_s$, $\dot{\hat{\boldsymbol{u}}}_o$	=	components of velocities in overlapping space
$\boldsymbol{x}_{c1}$, $\boldsymbol{x}_{c2}$	=	nonlinear coordinates along crack surface
$\boldsymbol{x}_h$	=	pristine structure coordinates
$\boldsymbol{x}_l$	=	coordinates that do not involve contact
$\boldsymbol{x}_r$	=	relative displacements between contact pairs
$\tilde{\boldsymbol{x}}_r$	=	relative displacements in contact direction
$\boldsymbol{x}_s$, $\boldsymbol{x}_o$	=	global coordinates
$\bar{\boldsymbol{x}}_s$, $\bar{\boldsymbol{x}}_o$	=	relative coordinates
α	=	relative coordinate transformation matrix
α	=	mass proportional damping coefficient
β_s, β_o	=	modified Craig-Bampton transformation matrices
$\tilde{\beta}_{o,r}$	=	portion of β_o with relative DOFs in contact direction
β	=	stiffness proportional damping coefficient
δ_i	=	mistuning value for ith blade
$\zeta_{s,j}$, $\zeta_{o,k}$	=	viscous damping ratios
$\theta_{s,j}$, $\theta_{o,k}$	=	phase angles in steady-state responses
$\boldsymbol{\Lambda}_0$	=	eigenvalue matrix of pristine structure
$\boldsymbol{\Lambda}_0^b$	=	eigenvalue matrix of tuned cantilever blade
$\boldsymbol{\Lambda}_i^{b,\delta}$	=	matrix of eigenvalue differences between tuned and mistuned blades
ν	=	Poisson's ratio
ρ	=	density
$\boldsymbol{\Phi}$	=	projection of overlapping space onto reduced space
$\boldsymbol{\Phi}_{\mathrm{CB}_c}$	=	crack acceleration modes
$\boldsymbol{\Phi}_{\mathrm{Full}}$	=	overlapping space
$\boldsymbol{\Phi}_{n,i}$	=	normal modes of ith sector
$\boldsymbol{\Phi}_s^m$, $\boldsymbol{\Phi}_o^m$	=	mode shapes of mistuned system in reduced coordinates
$\bar{\boldsymbol{\Phi}}_o^m$	=	transformed mode shapes of system in its open state
$\hat{\boldsymbol{\Phi}}_s^m$, $\hat{\boldsymbol{\Phi}}_o^m$	=	mode shapes in overlapping space
$\boldsymbol{\Psi}_c$	=	constraint modes
ψ	=	phase angle in steady-state responses
ω	=	excitation frequency

Presented as Paper 2019 at the 2019 AIAA SciTech Forum and Exposition, San Diego, CA, 7–11 January 2019; received 20 December 2018; revision received 20 May 2019; accepted for publication 20 May 2019; published online 25 June 2019.

*Fast Fellow, Department of Mechanical and Aerospace Engineering; tien.36@osu.edu.

†Graduate Student, Department of Mechanical and Aerospace Engineering; hu.629@osu.edu.

‡Assistant Professor, Department of Mechanical and Aerospace Engineering; dsouza.60@osu.edu (Corresponding Author).

$\omega_{s,j}$, $\omega_{o,k}$ = undamped natural frequencies
$\omega_{\mathrm{sd},j}$, $\omega_{\mathrm{od},k}$ = damped frequencies

Subscripts

i = sector number
j, k = mode numbers
o = open state
s = sliding state

Superscripts

b = cantilever blade
m = mistuned system
r = relative displacement

I. Introduction

ANALYSIS of the influence of cracks in cyclically symmetric systems such as bladed disks is important for design, failure analysis, and structural health monitoring in these systems. Predicting the dynamics of bladed disks is challenging for a variety of reasons: 1) complex geometry of modern turbines results in very high-dimensional computational models; 2) mistuning in these structures breaks the cyclic symmetry in these systems; 3) cracks further disrupt the symmetry in these systems; and 4) the breathing effect induced by cracks introduces a piecewise-linear nonlinearity into the system. To analyze the influence of cracks and mistuning on the dynamics of cyclic symmetric structures, an efficient method that can handle all of these challenges is required.

Bladed disks are typically designed to be cyclically symmetric because each disk-blade sector is supposed to be identical. However, there always exist small variations in structural properties among the sectors that stem from manufacturing tolerances, material deviations, and operational wear [1]. These random variations are referred to as blade mistuning. Modeling mistuning for cyclic symmetric structures is an active research area where many works have been published. Some early works employed lumped parameter models to analyze mistuning [2–6]. These simple models cannot accurately predict the response of modern industrial bladed disks. Therefore, several approaches have been developed to construct reduced-order models from representative high-dimensional finite element (FE) models. For instance, the subset of nominal modes (SNM) approach [7] uses a truncated set of normal modes of a tuned system because this serves as a good basis of the mistuned system when the mistuning is small. This idea is also employed in the fundamental model of mistuning (FMM) method [8] that is based on simplifying SNM for targeted bladed dominated mode families. Both the SNM and FMM method require eigen-decomposition of sector-level models of the stage by employing cyclic symmetry analysis. A similar idea is used in the component mode mistuning (CMM) approach [1] to model small mistuning in bladed disks. The CMM method is a very general modeling framework for cyclic symmetric structures that has recently been implemented in the commercial software ANSYS. Moreover, some recent works have been done to efficiently model large mistuning [9–11]. All of these reduced-order modeling techniques are developed for analyzing linear systems. A key feature of the most useful reduced-order modeling methods is the ability to use sector-level models and calculations, because the full-stage model may be too large to construct and analyze in industrial applications.

The piecewise-linear nonlinearity induced by cracks eliminates the use of efficient linear computational techniques. Thus, there are several methods based on linear transformations that have been developed to improve the efficiency of analyzing complex systems when nonlinearities are discrete, such as the Irons–Guyan reduction [12], the improved reduced system [13], the system equivalent reduction expansion process [14], multilevel substructuring [15,16], and component mode synthesis [17,18]. These linear approaches reduce the dynamics of the linear portion of the system while treating the localized nonlinearity as master degrees of freedom (DOFs). Recently, a new reduced-order modeling technique for complex cyclic symmetric structures with cracks, which is referred to as the X-X_r method [19], has been developed. This approach employs relative coordinates to describe the relative motion of the contacting surfaces and applies Craig–Bampton component modes synthesis (CB-CMS) [17] with cyclic analysis to reduce the rest of the system. The response of the reduced system can then be analyzed using nonlinear methods, such as alternating frequency/time (AFT) domain methods [20–26]. Although these AFT approaches are more efficient than traditional time integration [27], they still require iterative calculations in the time and frequency domain until the response converges. Thus, these methods are still computationally expensive, particularly as the number of nonlinear DOFs increases.

Recently, several linear methods referred to as the bilinear amplitude approximation (BAA) method [28,29] and the hybrid symbolic-numeric computational (HSNC) method [30,31] have been developed to efficiently compute the dynamics of piecewise-linear nonlinear systems. These methods use the fact that the nonlinear response of these systems can be obtained by combining all the responses in each time interval where the system behaves linearly. The BAA method, in particular, is developed for conducting parametric analyses of these systems because it can efficiently analyze the influence of parameter changes on the steady-state response. The BAA approach approximates the vibrational response of piecewise-linear nonlinear systems by combining the responses in their two specific linear states: the fully open state and the fully sliding state. A single vibration cycle can be constructed by coupling these linear responses using specialized boundary conditions at the transition. The BAA method is several order of magnitude faster than nonlinear methods because it is based on linear calculations of a reduced subset of linear modes. Furthermore, the method can be incorporated with the X-X_r approach to efficiently predict the dynamics of complex cyclic symmetric structures with cracks [32].

Several methods mentioned above have been developed to handle many challenges individually. This work will modify and combine the CMM, X-X_r, and BAA method for the first time to enable the efficient construction and analysis of mistuned bladed disks with cracks using sector-level calculations and linear analysis tools. The effects of the mistuning pattern and crack size on the dynamics are statistically investigated using the proposed method.

II. Methodology

In this section, a new computational framework that combines the X-X_r, CMM, and BAA methods to approximate the forced response of bladed disks with mistuning and cracks is proposed. The new method is able to construct a reduced-order model (ROM) of these systems using sector-level calculations and efficiently approximate the nonlinear response using linear techniques.

Consider an FE model of a bladed disk with N sectors shown in Fig. 1a. In this case the first sector contains the blade with a crack schematically shown in Fig. 1b. Because of the breathing effect of the crack, cracked surfaces of an elastic structure typically undergo three different states: 1) fully sliding (i.e., complete contact), 2) fully open (i.e., no contact), and 3) partially open (i.e., partial contact between the surfaces). Moreover, cracked structures usually respond periodically if the system is excited by periodic forces and the partially open state generally lasts a much shorter time interval than the fully sliding state and the fully open state. Thus, the proposed method is developed for the case where vibration cycles can be approximated well by the fully sliding and fully open states only; that is, the partially open state has a negligible effect on the overall motion. If a gap/prestress does not exist between the contact surfaces, the equations of motion for the system in its sliding state and open state can be expressed as

$$\begin{aligned} \boldsymbol{M}_s\ddot{\boldsymbol{x}}_s(t) + \boldsymbol{C}_s\dot{\boldsymbol{x}}_s(t) + \boldsymbol{K}_s\boldsymbol{x}_s(t) &= \boldsymbol{F}(t), \\ \boldsymbol{M}_o\ddot{\boldsymbol{x}}_o(t) + \boldsymbol{C}_o\dot{\boldsymbol{x}}_o(t) + \boldsymbol{K}_o\boldsymbol{x}_o(t) &= \boldsymbol{F}(t) \end{aligned} \tag{1}$$

where $\boldsymbol{M}$, $\boldsymbol{C}$, and $\boldsymbol{K}$ are the mass matrix, damping matrix, and stiffness matrix of the entire structure, respectively; the subscript s

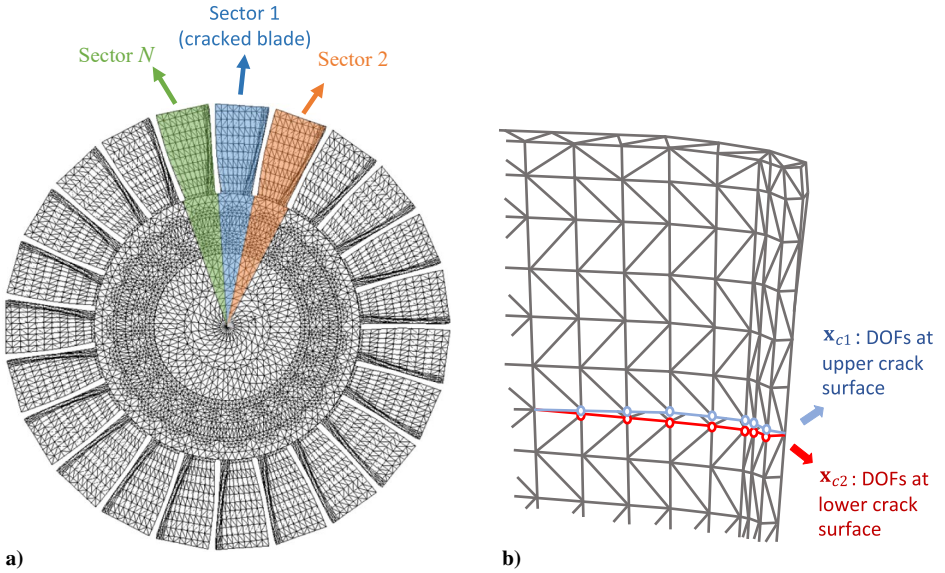

Fig. 1 a) Finite element model of the bladed disk with a cracked blade. b) Close-up of the blade with a crack.

refers to the sliding state; the subscript o refers to the open state; and $\boldsymbol{F}(t)$ is the harmonic force with frequency ω. Note that the contact stiffness and damping are applied when the bladed disk is in its fully sliding state to reduce the penetration or separation in the contact direction between each contact pair. The contact direction is defined as the direction normal to the crack surfaces.

To facilitate the construction of the ROM, the coordinates are reordered and expressed as

$$\boldsymbol{x} = [\boldsymbol{x}_{c1}^T \quad \boldsymbol{x}_{c2}^T \quad \boldsymbol{x}_l^T]^T \tag{2}$$

where $\boldsymbol{x}_{c1}$ and $\boldsymbol{x}_{c2}$ represent the nonlinear DOFs (i.e., the contacting DOFs) along the crack surface shown in Fig. 1b, and $\boldsymbol{x}_l$ are the rest of the DOFs in the entire structure. The system matrices that correspond to this coordinate system can be partitioned as

$$\boldsymbol{M} = \begin{bmatrix} \boldsymbol{M}_{c1,c1} & \boldsymbol{M}_{c1,c2} & \boldsymbol{M}_{c1,l} \\ \boldsymbol{M}_{c1,c2}^T & \boldsymbol{M}_{c2,c2} & \boldsymbol{M}_{c2,l} \\ \boldsymbol{M}_{c1,l}^T & \boldsymbol{M}_{c2,l}^T & \boldsymbol{M}_{l,l} \end{bmatrix},$$

$$\boldsymbol{C} = \begin{bmatrix} \boldsymbol{C}_{c1,c1} & \boldsymbol{C}_{c1,c2} & \boldsymbol{C}_{c1,l} \\ \boldsymbol{C}_{c1,c2}^T & \boldsymbol{C}_{c2,c2} & \boldsymbol{C}_{c2,l} \\ \boldsymbol{C}_{c1,l}^T & \boldsymbol{C}_{c2,l}^T & \boldsymbol{C}_{l,l} \end{bmatrix},$$

$$\boldsymbol{K} = \begin{bmatrix} \boldsymbol{K}_{c1,c1} & \boldsymbol{K}_{c1,c2} & \boldsymbol{K}_{c1,l} \\ \boldsymbol{K}_{c1,c2}^T & \boldsymbol{K}_{c2,c2} & \boldsymbol{K}_{c2,l} \\ \boldsymbol{K}_{c1,l}^T & \boldsymbol{K}_{c2,l}^T & \boldsymbol{K}_{l,l} \end{bmatrix} \tag{3}$$

The X-X_r method [19] can then be applied to reduce the system. The reduction process is summarized as follows:

1) Perform a coordinate transformation (α transformation) so that the motion along the crack surface is described in relative coordinates $\bar{\boldsymbol{x}}$.

2) Compute the constraint modes $\boldsymbol{\Psi}_c$, crack acceleration modes $\boldsymbol{\Phi}_{\mathrm{CB}_c}$, and normal modes of the pristine system $\boldsymbol{\Phi}_{n,i}$ to construct the Craig-Bampton transformation matrix $\boldsymbol{\beta}$. Note that $\boldsymbol{\Psi}_c$ is assumed to be a localized deformation. It is considered to be nonzero only at the sector with a crack.

3) The ROM of the entire system is then obtained by applying the $\boldsymbol{\beta}$ transformation using subsets of the crack acceleration modes and the normal modes of the pristine system. The selection of these modes is based upon the frequency range of interest.

The X-X_r reduction process is described in detail in Appendix A and the reduced equations of motion of the system can be expressed as

$$\begin{aligned} &\boldsymbol{M}_{\mathrm{ROM},s}\ddot{\boldsymbol{u}}_s(t) + \boldsymbol{C}_{\mathrm{ROM},s}\dot{\boldsymbol{u}}_s(t) + \boldsymbol{K}_{\mathrm{ROM},s}\boldsymbol{u}_s(t) = \boldsymbol{F}_{\mathrm{ROM},s}(t), \\ &\boldsymbol{M}_{\mathrm{ROM},o}\ddot{\boldsymbol{u}}_o(t) + \boldsymbol{C}_{\mathrm{ROM},o}\dot{\boldsymbol{u}}_o(t) + \boldsymbol{K}_{\mathrm{ROM},o}\boldsymbol{u}_o(t) = \boldsymbol{F}_{\mathrm{ROM},o}(t) \end{aligned} \tag{4}$$

where

$$\boldsymbol{M}_{\mathrm{ROM}} = \begin{bmatrix} \boldsymbol{M}_{11} & \boldsymbol{M}_{12} & \boldsymbol{M}_{13} \\ \boldsymbol{M}_{12}^T & \boldsymbol{M}_{22} & \boldsymbol{M}_{23} \\ \boldsymbol{M}_{13}^T & \boldsymbol{M}_{23}^T & \boldsymbol{M}_{33} \end{bmatrix},$$

$$\boldsymbol{C}_{\mathrm{ROM}} = \begin{bmatrix} \boldsymbol{C}_{11} & \boldsymbol{C}_{12} & \boldsymbol{C}_{13} \\ \boldsymbol{C}_{12}^T & \boldsymbol{C}_{22} & \boldsymbol{C}_{23} \\ \boldsymbol{C}_{13}^T & \boldsymbol{C}_{23}^T & \boldsymbol{C}_{33} \end{bmatrix},$$

$$\boldsymbol{K}_{\mathrm{ROM}} = \begin{bmatrix} \boldsymbol{K}_{11} & \boldsymbol{K}_{12} & \boldsymbol{K}_{13} \\ \boldsymbol{K}_{12}^T & \boldsymbol{K}_{22} & \boldsymbol{K}_{23} \\ \boldsymbol{K}_{13}^T & \boldsymbol{K}_{23}^T & \boldsymbol{K}_{33} \end{bmatrix} \tag{5}$$

Note that $\boldsymbol{M}_{\mathrm{ROM}}$, $\boldsymbol{C}_{\mathrm{ROM}}$, and $\boldsymbol{K}_{\mathrm{ROM}}$ are the system matrices in the reduced space and $\boldsymbol{F}_{\mathrm{ROM}}$ is the reduced forcing vector. The submatrices with subscripts 11, 12, 13, 22, and 23 are associated with the sector with a crack (the *first* sector was chosen as the sector with a crack in this paper) and the submatrices with subscript 33 are associated with the pristine component of the entire bladed disk (i.e., the structure without any crack). Note that $\boldsymbol{M}_{33} = \boldsymbol{I}$ and $\boldsymbol{K}_{33} = \boldsymbol{\Lambda}_0$, where $\boldsymbol{\Lambda}_0$ is the eigenvalue matrix of the pristine bladed disk. Explicit expressions of all the submatrices in Eq. (5) can be found in Appendix A. Note that these submatrices can be computed using sector-level calculations; thus, sector-level models are sufficient to construct the ROM of the entire bladed disk, and this leads to great computational savings.

Next, the CMM method [1] is modified and applied to the ROM to account for the mistuning of the bladed disk. The CMM method assumes that the mistuning is in the blades and that the mistuning level is small, and so the mistuned normal modes can be expressed using a subset of normal modes of the tuned system. In this work, mistuning is modeled in the blade portion of the bladed disk by introducing different Young's modulus for each blade $E_i = E_0(1 + \delta_i)$, where E_0 is Young's modulus for the tuned system and δ_i is the dimensionless mistuning value for the ith blade. The mistuning pattern of each blade can be efficiently assigned in the reduced space by modifying the reduced stiffness matrix

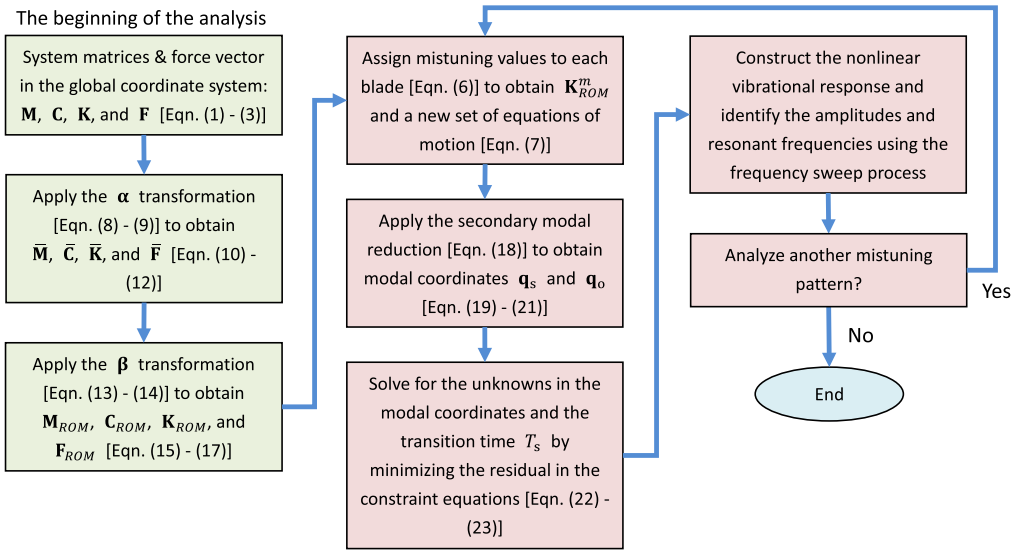

Fig. 2 The overall analysis process for bladed disks with mistuning and cracks.

$$\boldsymbol{K}^m_{\mathrm{ROM}} = \begin{bmatrix} \boldsymbol{K}^m_{11} & \boldsymbol{K}^m_{12} & \boldsymbol{K}^m_{13} \\ \boldsymbol{K}^{mT}_{12} & \boldsymbol{K}^m_{22} & \boldsymbol{K}^m_{23} \\ \boldsymbol{K}^{mT}_{13} & \boldsymbol{K}^{mT}_{23} & \boldsymbol{K}^m_{33} \end{bmatrix} = \begin{bmatrix} (1+\delta_1)\boldsymbol{K}_{11} & (1+\delta_1)\boldsymbol{K}_{12} & (1+\delta_1)\boldsymbol{K}_{13} \\ (1+\delta_1)\boldsymbol{K}_{12}{}^T & (1+\delta_1)\boldsymbol{K}_{22} & (1+\delta_1)\boldsymbol{K}_{23} \\ (1+\delta_1)\boldsymbol{K}_{13}{}^T & (1+\delta_1)\boldsymbol{K}_{23}{}^T & \boldsymbol{\Lambda}_0 + \sum_{i=1}^{N} \boldsymbol{p}_i^{bT} \boldsymbol{\Lambda}_i^{b,\delta} \boldsymbol{p}_i^b \end{bmatrix} \tag{6}$$

where $\boldsymbol{\Lambda}_i^{b,\delta}$ is the diagonal matrix that includes the eigenvalue difference between the tuned and mistuned system and $\boldsymbol{p}_i^b$ includes the modal participation factors of the ith blade, which is the contribution of each tuned mode for the system. Note that $\boldsymbol{\Lambda}_i^{b,\delta} = \delta_i \boldsymbol{\Lambda}_0^b$, where $\boldsymbol{\Lambda}_0^b$ is the eigenvalue matrix of the tuned cantilever blade. The submatrices with subscripts 11, 12, 13, 22, and 23 are associated with the sector with a crack; thus, the mistuned stiffness for these parts must be approximated by scaling the submatrices of the tuned system by the appropriate mistuning, namely, $(1+\delta_1)$. If the damping is proportional to the mass and stiffness of the system ($\boldsymbol{C}^m_{\mathrm{ROM}} = \alpha \boldsymbol{M}_{\mathrm{ROM}} + \beta \boldsymbol{K}^m_{\mathrm{ROM}}$), the equations of motion for the mistuned system in its sliding and open states can be written as

$$\begin{aligned} &\boldsymbol{M}_{\mathrm{ROM},s}\ddot{\boldsymbol{u}}_s(t) + (\alpha \boldsymbol{M}_{\mathrm{ROM},s} + \beta \boldsymbol{K}^m_{\mathrm{ROM},s})\dot{\boldsymbol{u}}_s(t) + \boldsymbol{K}^m_{\mathrm{ROM},s}\boldsymbol{u}_s(t) \\ &\quad = \boldsymbol{F}_{\mathrm{ROM},s}(t), \\ &\boldsymbol{M}_{\mathrm{ROM},o}\ddot{\boldsymbol{u}}_o(t) + (\alpha \boldsymbol{M}_{\mathrm{ROM},o} + \beta \boldsymbol{K}^m_{\mathrm{ROM},o})\dot{\boldsymbol{u}}_o(t) + \boldsymbol{K}^m_{\mathrm{ROM},o}\boldsymbol{u}_o(t) \\ &\quad = \boldsymbol{F}_{\mathrm{ROM},o}(t) \end{aligned} \tag{7}$$

Note that Eq. (7) for different mistuning patterns can be efficiently constructed because the mistuning values can be applied in the ROM instead of the full FE model. This enables the efficient creation of different ROMs of bladed disk with cracks and different mistuning patterns.

Next, the BAA method [29,32] is applied to approximate the nonlinear response of the system. The BAA method uses the fact that a nonlinear vibrational cycle for systems with cracks can often be approximated well by combining the responses of the system in its fully sliding and fully open states. A nonlinear optimization solver is used to numerically solve for the unknown coefficients in the linear responses by minimizing the residual of a set of constraint equations derived for coupling these linear responses. The details of the BAA method are described in Appendix B and the response approximation process is summarized as follows:

1) A secondary modal reduction $\boldsymbol{u}_s = \boldsymbol{\Phi}^m_s \boldsymbol{q}_s$ and $\boldsymbol{u}_o = \boldsymbol{\Phi}^m_o \boldsymbol{q}_o$ is carried out on Eq. (7) to project the equations of motion along subspaces constructed by subsets of mode shapes grouped in $\boldsymbol{\Phi}^m_s$ and $\boldsymbol{\Phi}^m_o$, where $\boldsymbol{\Phi}^m_s$ and $\boldsymbol{\Phi}^m_o$ represent the modes that dominate the motion of the mistuned structure in its sliding state and open state, respectively.

2) The modal coordinates $\boldsymbol{q}_s$ and $\boldsymbol{q}_o$ can then be expressed as combinations of the linear transient response and the linear steady-state response listed in Eq. (B4).

3) A set of specialized constraint equations is derived and a nonlinear optimization solver is used to numerically solve for the transition time T_s and unknown coefficients in Eq. (B4) by minimizing the residual of the constraint equations, where T_s is the time span where the system stays in the sliding state. The system response is assumed to have the same period as the excitation force and switches from the sliding state to the open state at $t = T_s$.

4) One steady-state nonlinear vibrational cycle can then be constructed using the physical displacements $\boldsymbol{x}_s$, $\boldsymbol{x}_o$, and the transition time T_s, where $\boldsymbol{x}_s = \boldsymbol{\alpha}\boldsymbol{\beta}_s \boldsymbol{\Phi}^m_s \boldsymbol{q}_s$ is the physical displacement of the system in its sliding state and $\boldsymbol{x}_o = \boldsymbol{\alpha}\boldsymbol{\beta}_o \boldsymbol{\Phi}^m_o \boldsymbol{q}_o$ is the physical displacement of the system in its open state.

Finally, the amplitudes and resonant frequency can be efficiently identified using a frequency sweep process over the chosen frequency range. The nonlinear forced response can be quickly obtained because the unknown coefficients in Eq. (B4) can be efficiently solved using the coefficients solved in the previous frequency point as initial values for the nonlinear optimization solver (an appropriate choice of initial values for the first frequency is needed to obtain a physically valid solution [29]). Furthermore, mistuning values can be directly assigned to the ROM; thus, the effects of numerous mistuning patterns and levels that integrate with different crack sizes can be efficiently analyzed for the bladed disk with cracks. The overall analysis process is summarized in Fig. 2.

III. Results

The FE model of the mistuned bladed disk studied in this work is shown in Fig. 3a. The bladed disk has 23 blades, and one of them has a crack. The Young's modulus for the system is $E_0 = 104.5$ GPa, the Poisson's ratio is $\nu = 0.342$, and the density is $\rho = 9224$ kg/m^3. Note that the damping matrix is proportional to the stiffness matrix by setting $\alpha = 0$ and $\beta = 7 \times 10^{-7}$. The full FE model contains 201,802 midside-node elements. Engine order (EO) excitations are applied to the structure at the nodes indicated by arrows in Fig. 3a for the forced response calculations. The EO excitation is the traveling wave excitation caused by disturbances in the flow field [33]. The forces applied to each blade have the same amplitude with different phase angles that are determined by the number of obstructions in the flow

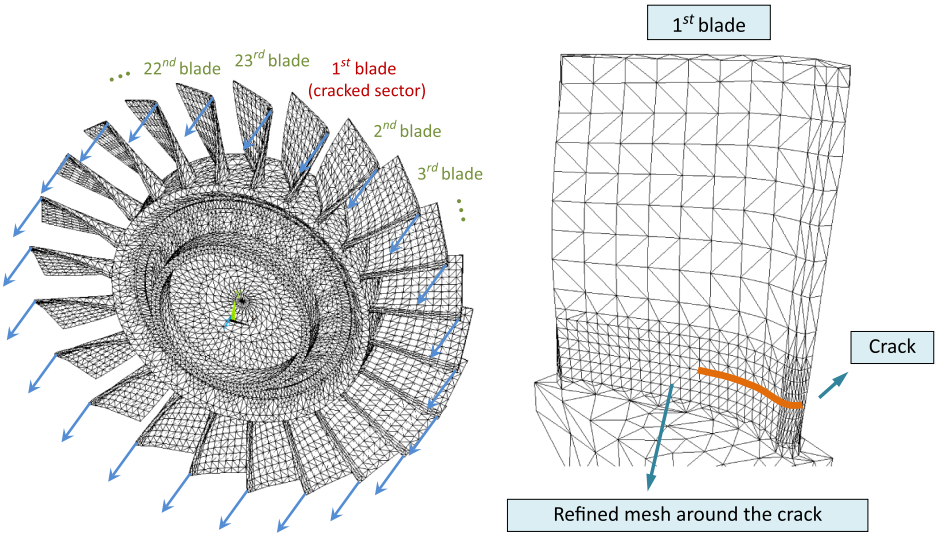

Fig. 3 a) Finite element model of the mistuned bladed disk with a cracked blade and excitation forces. b) Close-up of the blade with a crack.

field. In this work, the EO11 excitation is applied to one tip node along each blade in the axial direction with an amplitude of 10 N. It is assumed that the crack is located at the leading edge on the pressure side of the first blade and its width is approximately two-thirds of the blade thickness as shown in Fig. 3b. Note that a refined mesh is used in the area around the crack. The models with different crack lengths and mistuning patterns are then analyzed using the proposed method.

A. Linear and Nonlinear Analysis

The nonlinear response obtained using the proposed method is compared with the FE solution computed using time integration and linear responses of the corresponding linear models (i.e., the system that always stays in its fully sliding state and the system that always stays in its fully open state). The response within a frequency range that contains the first mode family is studied in this work. Note that the length of the crack is approximately one-half of the chord in this analysis. A large crack is analyzed first to demonstrate the effectiveness of the integrated method, which uses linear analysis tools, when there is a strong nonlinearity present.

First, a ROM that is accurate over the first five mode families is created using the X-X_r reduction process. The ROM has 566 DOFs, including 390 DOFs on the crack surfaces (i.e., there are 130 contact pairs). A zero mean 4% standard deviation (SD) stiffness mistuning is then applied to the ROM. It is observed that the linear response of each blade is dominated by different modes in the chosen frequency range; thus, the entire first mode family is selected in the secondary modal reduction in this work. Note that the modal selection process is more involved for the tuned system because only a subset of modes in the mode family respond to the excitation. A careful selection for the modes is required [32]. The approximated nonlinear response is then obtained by numerically solving for the unknowns in the constraint equations and the forced response can be computed using the frequency sweep process.

Next, traditional FE analysis is performed to validate the nonlinear response obtained from the proposed method. The FE solution is performed using the commercial software ANSYS. To speed up the simulation, the substructuring analysis is first employed to reduce the required computational cost. The substructuring analysis is conducted using CB-CMS [17] by retaining the elements in the refined mesh area while condensing all other elements into superelements. The transient dynamic analysis (time integration) is then used to compute the time history of the system at a specific frequency. Note that the Newmark method [34] is used in the transient dynamic analysis. Furthermore, the linear responses of the structure with a crack in its linear states are computed using the ROM created using the X-X_r method [i.e., the responses for the sliding and open systems given in Eq. (7)].

The tip displacement amplitudes of the sector with a crack and its adjacent sectors computed using the proposed method and FE analysis are plotted and compared in Fig. 4. The linear responses of the system in its fully sliding state and fully open state are also plotted in the figures. It is shown that the proposed method is able to capture the resonant frequencies and amplitudes of all the blades at a fraction of the computational cost. For the proposed method, the average CPU time required to compute the nonlinear response for a specific frequency using a workstation with Intel i7 processors (3.6 GHz) is 0.49 s. By contrast, FE analysis requires approximately 12 h to integrate to a steady-state response even with the FE model size being reduced significantly using substructruing analysis. The proposed method requires only 1.13×10^{-3}% of the CPU time of the substructuring-transient dynamic analysis to obtain the approximation. Furthermore, it is observed that there is a noticeable difference among the linear responses and the nonlinear response at the first sector and the second sector (the sector with a crack and its adjacent sector) in the case studied. The linear analysis is not able to capture the change in the dynamics caused by the localized crack effect. Thus, the proposed method is a valuable tool to efficiently investigate the system with cracks and different mistuning patterns.

B. Effect of Crack Length on the Dynamics of the Mistuned Bladed Disk

To analyze the effect of the crack on the dynamics of the bladed disk, the forced responses of the pristine structure and structures with different crack lengths are compared and plotted in Fig. 5. The response of the pristine structure is obtained by computing the linear response from a ROM constructed using the standard CMM approach. The nonlinear responses computed using the proposed method for the cases where the crack length is approximately one-ninth, one-fourth, and one-half of the chord are compared with the response of the pristine structure and validated using FE solutions. The blade-tip responses of the 1st blade and its adjacent blades (2nd, 3rd, 22nd, and 23rd) are shown in Figs. 5a–5e, respectively. Note that the same set of mistuning values with zero mean and 4% SD is used for all the cases studied. Figure 5 shows that the nonlinear response computed using the proposed method agrees well with the FE solution for all the cases. Note that significant changes in the resonant frequency and amplitudes can be observed at the blade with a crack; furthermore, a noticeable change in the response can also be found at the 2nd blade for this particular mistuning pattern. The nonlinear response of the system with a crack asymptotically approaches the response of the pristine system as the crack length is reduced. However, the presence of the crack does not significantly impact the dynamics of the rest of the pristine sectors in this case. Thus, the

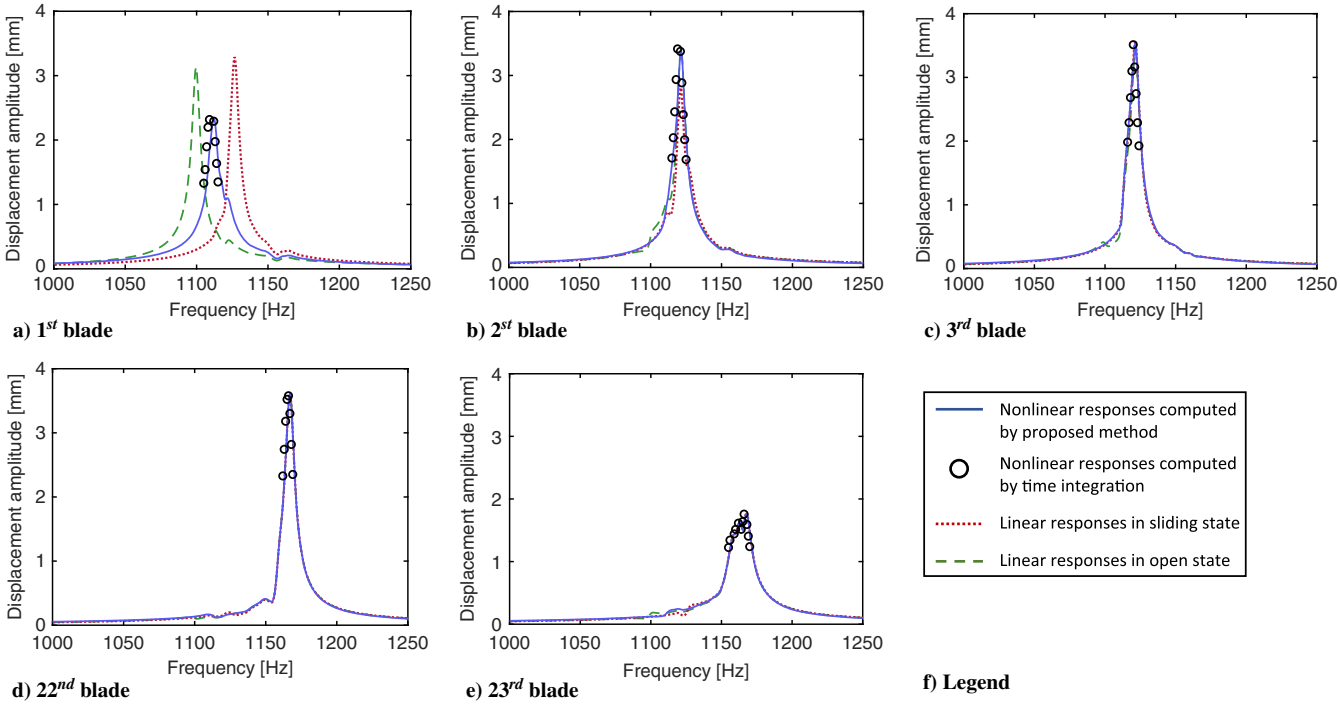

Fig. 4 Comparison of nonlinear vibration responses obtained using the proposed method and time integration.

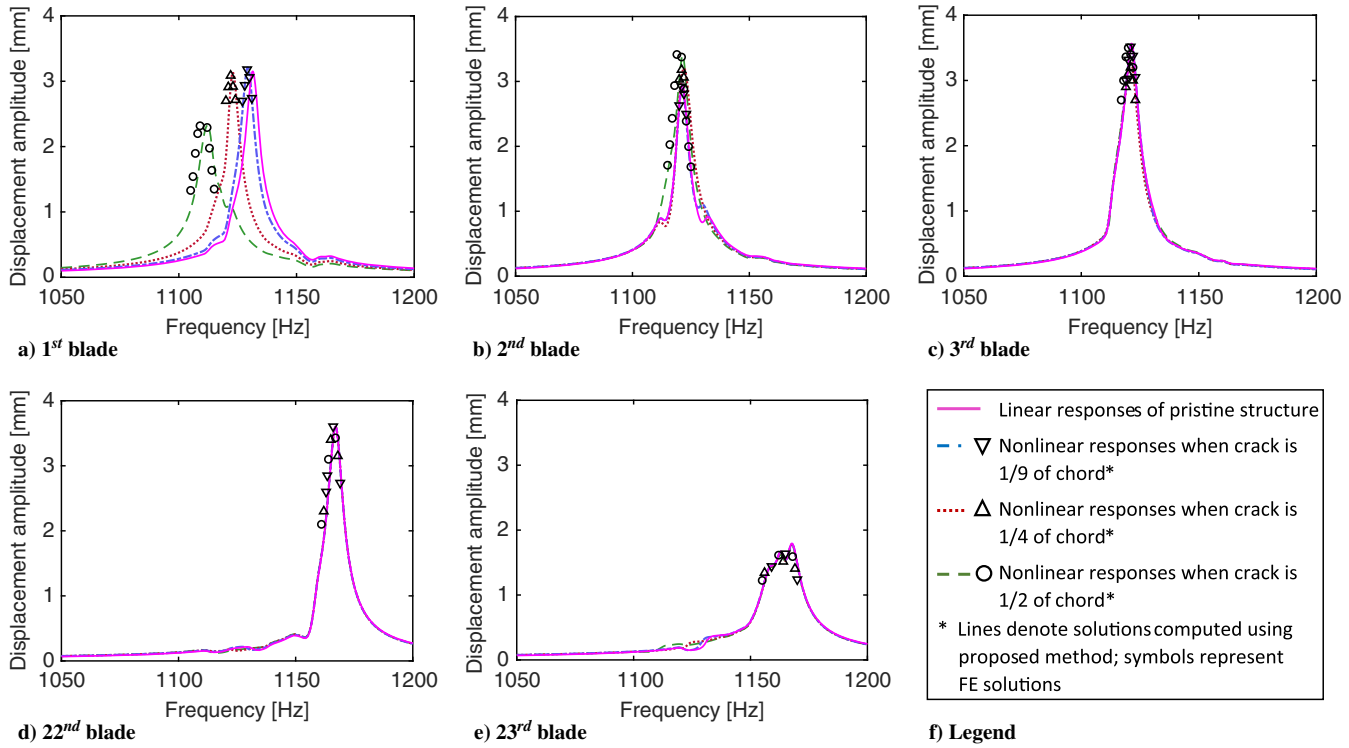

Fig. 5 Comparison of the vibration responses for the pristine bladed disk and bladed disks with cracks of different lengths and the same mistuning pattern.

presence of the crack only results in a localized effect and does not alter the overall dynamic behavior caused by the existing mistuning pattern.

C. Effect of Mistuning on the Dynamics of the Bladed Disk with a Crack

The effect of different mistuning patterns on the response of the system is investigated in this section. A few sets of mistuning values δ_i with zero mean and 4% SD are randomly generated. Note that these mistuning values can be directly applied to the ROM in the reduced space, and hence there is no need to reconstruct the ROM, which occupies most of the required CPU time. The nonlinear response of the blade with a crack and the maximum response among all the blades computed using the proposed method for three different mistuning patterns are plotted in Fig. 6. Moreover, these nonlinear responses are validated with FE solutions. It is observed that the nonlinear responses obtained by the proposed method agrees with the FE solutions for all the mistuning cases studied. The response at the

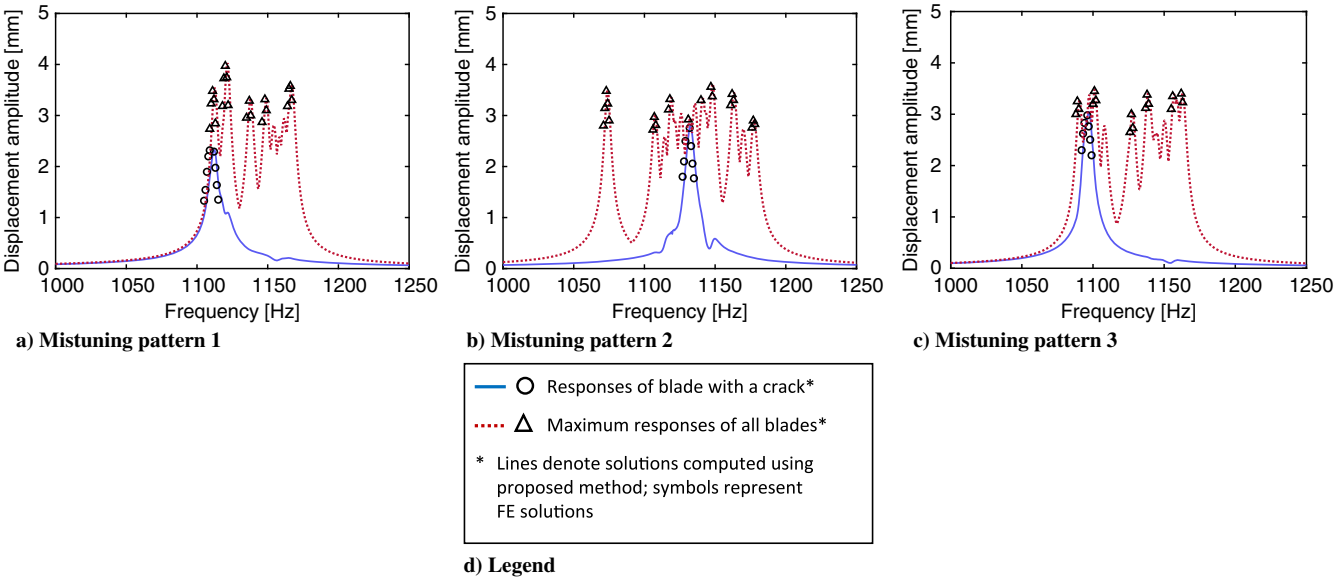

Fig. 6 The response of the blade with a crack and the maximum response among all the blades for three different mistuning patterns.

sector with a crack and the maximum response both shift significantly as the mistuning pattern changes. Furthermore, the presence of random mistuning results in nonpredictable changes in the dynamics of bladed disks with cracks. To understand the coupling effect of the presence of cracks and mistuning on bladed disks, a further statistical analysis is required.

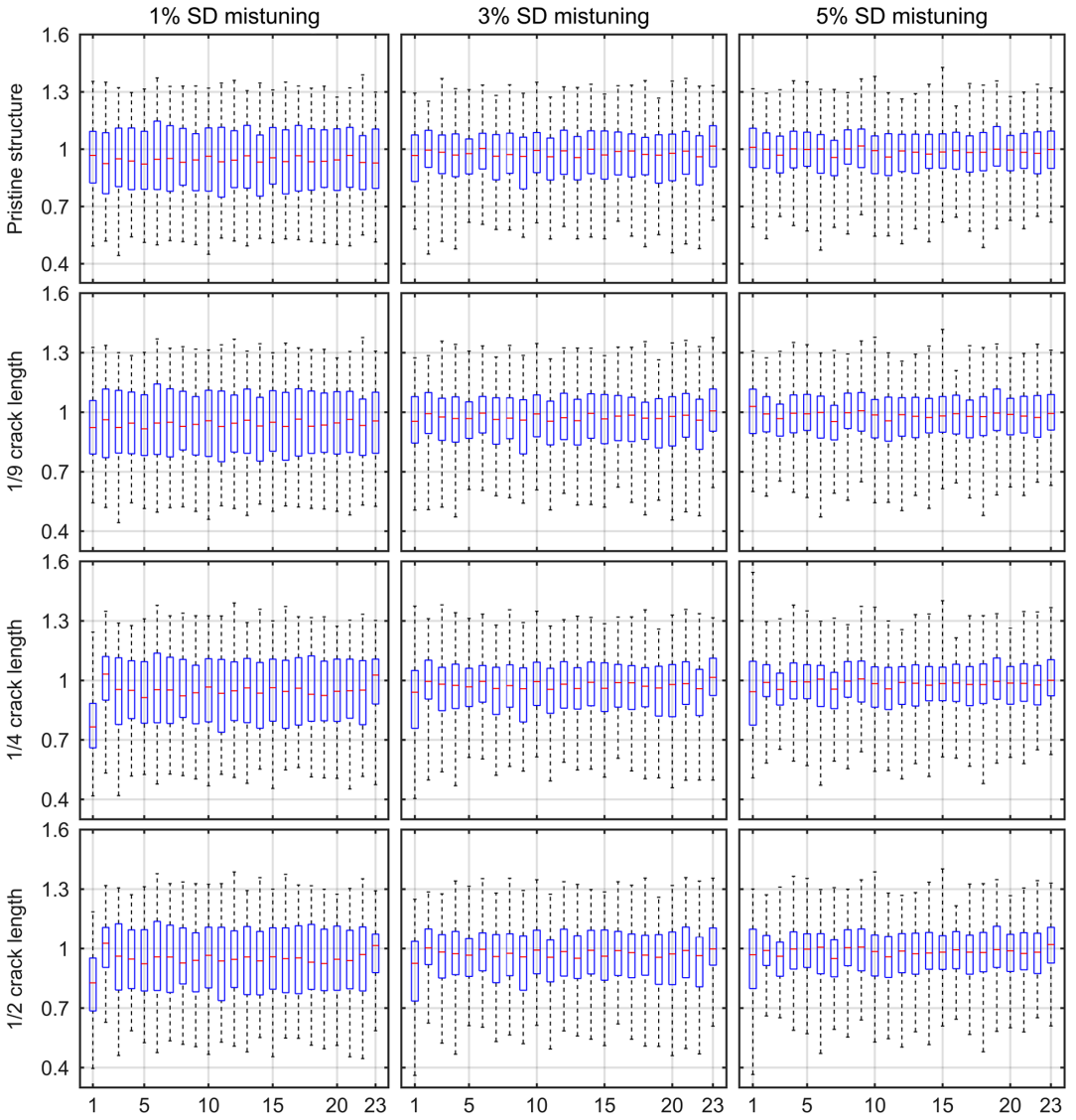

Fig. 7 Box plots of the normalized amplitude values. Box plots indicate maximum, minimum, mean, first quartile, and third quartile values.

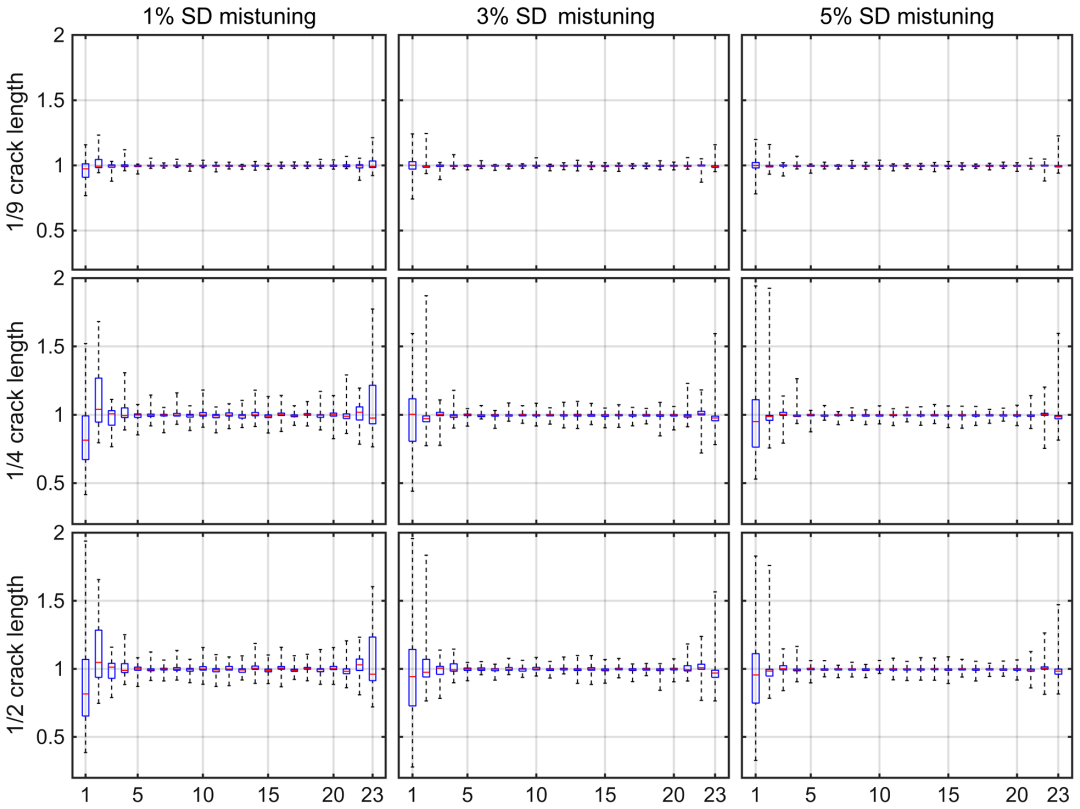

Fig. 8 Box plots of the rescaled amplitude values. Box plots indicate maximum, minimum, mean, first quartile, and third quartile values.

D. Statistical Analysis

With the proposed method validated, it is now used to investigate the statistical properties of the dynamics of bladed disks with varying crack length and mistuning pattern. The nonlinear forced response of the structure is computed for three mistuning levels (zero mean 1%, zero mean 3%, and zero mean 5% SD mistuning). Note that 150 randomly generated mistuning patterns are applied to the ROM for each mistuning level, and the responses of the pristine structure and the structure with three different crack lengths (approximately one-ninth of the chord, one-fourth of the chord, and one-half of the chord) are computed for each mistuning pattern. The maximum amplitudes within the frequency range that contains the first mode family are recorded and are normalized with respect to the amplitude of the pristine structure without mistuning. The statistical properties of the normalized amplitudes at each blade are shown in Fig. 7 using box plots. Each box plot displays the minimum, first quartile, median, third quartile, and maximum amplitude values at each blade from 150 mistuning calculations. In these plots, the ends of the whiskers represent the minimum and maximum amplitude values; the ends of the boxes represent the first quartile and third quartile amplitude values; the bands inside the boxes represent the median amplitude values. The horizontal axis represents blade number and the vertical axis represents the normalized amplitude (amplification factor for a given sector). Note that the box plots in the same column represent the results computed using the same set of mistuning patterns. Each column has the specified mistuning level, and each row has the specified crack length.

Figure 7 shows that the interquartile ranges of the normalized amplitude values of the pristine structure reduce as the mistuning level grows. This matches another study done by Bladh et al. [35], where variation of the pristine blade amplitude has a local maximum at 1% SD mistuning. It is observed that this trend still holds for pristine sectors when a crack is present at the first blade. However, the interquartile range of the normalized amplitude values at the blade with a crack exhibits a different pattern when the mistuning level changes. For the cases where the crack length is one-fourth and one-half of the chord, the variation of the amplitude values at the blade with a crack is getting higher when the mistuning level increases. This results in a phenomenon that the variation of the normalized amplitude values of the blade with a crack is relatively larger than that of other pristine sectors when the crack length and mistuning level are both large. Note that the largest amplification factor occurs in the blade with a crack one-fourth the chord length with 5% SD in mistuning. This largest amplification occurs in the blade with a crack due to the interaction of mistuning and the crack.

Next, changes in the dynamics of the mistuned bladed disk caused by crack propagation are statistically investigated. For a given mistuning pattern, the blade amplitude of the structure with a crack is rescaled by dividing it by the amplitude of the structure without a crack, but with the same mistuning pattern. The rescaled amplitude represents the amplification of the response due to the presence of the crack with a given mistuning pattern. The box plots of the rescaled amplitude values computed from 150 ROMs with different mistuning patterns and crack conditions are shown in Fig. 8. In these plots, the horizontal axis represents blade number and the vertical axis represents the rescaled amplitude. Note that the box plots in the same column represent the results computed using the same set of mistuning patterns. Each column has the specified mistuning level, and each row has the specified crack length. Figure 8 shows that the variation in the rescaled amplitudes of all the blades grow when the crack length increases. However, significant variation can only be observed at the blade with a crack and its adjacent blades. The presence of the crack results in a significantly localized variation in the area near the crack. In this case, the mistuning level has no significant impact on the amplification of the response.

IV. Conclusions

An efficient computational framework that combines several previously developed methods (X-X_r, component mode mistuning (CMM), and bilinear amplitude approximation (BAA)) is introduced in this paper. The new technique is developed to approximate the nonlinear forced response of cyclic symmetric structures with mistuning and cracks. The method is shown to be accurate and is several orders of magnitude faster than traditional time integration. Statistical analyses of the response of complex cyclic systems with

piecewise-linear nonlinearities are enabled, for the first time, by this efficient computational framework.

The dynamics of bladed disks with cracks and mistuning are studied in this work. The reduced-order model (ROM) of the structure is constructed using the X-X_r method. The mistuning values are then applied to the ROM using the modified CMM approach. The nonlinear vibrational response is approximated using the BAA method and the resonant frequency and amplitudes are identified using a frequency sweep process. The effects of different mistuning patterns and crack sizes on the dynamics of bladed disks are analyzed. The statistical properties of the system are also discussed.

Appendix A: X-X_r Method

This section details the construction of a ROM of a bladed disk with a crack using the X-X_r approach [19]. Note that all the system matrices discussed in this appendix correspond to the tuned system. Mistuning will be directly assigned to the ROM created using the X-X_r method.

First, a coordinate transformation is applied to the global coordinates [Eq. (2)] so that the motion at the crack surfaces can be described using relative coordinates

$$\boldsymbol{x} = \begin{bmatrix} \boldsymbol{x}_{c1} \\ \boldsymbol{x}_{c2} \\ \boldsymbol{x}_l \end{bmatrix} = \boldsymbol{\alpha} \begin{bmatrix} \boldsymbol{x}_r \\ \boldsymbol{x}_{c2} \\ \boldsymbol{x}_l \end{bmatrix} = \boldsymbol{\alpha} \begin{bmatrix} \boldsymbol{x}_r \\ \boldsymbol{x}_h \end{bmatrix} = \boldsymbol{\alpha}\bar{\boldsymbol{x}} \tag{A1}$$

where $\boldsymbol{x}_r = \boldsymbol{x}_{c1} - \boldsymbol{x}_{c2}$ describes the relative displacements between each contact pair, $\boldsymbol{x}_h = [\boldsymbol{x}_{c2}^T, \boldsymbol{x}_l^T]^T$ represents the DOFs of the corresponding pristine structure where the crack is not present, and the transformation matrix α is defined as

$$\alpha = \begin{bmatrix} \boldsymbol{I} & \boldsymbol{I} & \boldsymbol{0} \\ \boldsymbol{0} & \boldsymbol{I} & \boldsymbol{0} \\ \boldsymbol{0} & \boldsymbol{0} & \boldsymbol{I} \end{bmatrix} \tag{A2}$$

After applying the transformation to Eq. (1), a new set of equations of motion using the relative coordinates can be obtained:

$$\begin{aligned} \bar{\boldsymbol{M}}_s \ddot{\bar{\boldsymbol{x}}}_s(t) + \bar{\boldsymbol{C}}_s \dot{\bar{\boldsymbol{x}}}_s(t) + \bar{\boldsymbol{K}}_s \bar{\boldsymbol{x}}_s(t) &= \bar{\boldsymbol{F}}(t), \\ \bar{\boldsymbol{M}}_o \ddot{\bar{\boldsymbol{x}}}_o(t) + \bar{\boldsymbol{C}}_o \dot{\bar{\boldsymbol{x}}}_o(t) + \bar{\boldsymbol{K}}_o \bar{\boldsymbol{x}}_o(t) &= \bar{\boldsymbol{F}}(t) \end{aligned} \tag{A3}$$

where

$$\begin{aligned} \bar{\boldsymbol{M}} &= \boldsymbol{\alpha}^T \boldsymbol{M} \alpha = \begin{bmatrix} \bar{\boldsymbol{M}}_{\boldsymbol{x}_r} & \bar{\boldsymbol{M}}_{\boldsymbol{x}_r,\boldsymbol{x}_h} \\ \bar{\boldsymbol{M}}_{\boldsymbol{x}_r,\boldsymbol{x}_h}^T & \bar{\boldsymbol{M}}_{\boldsymbol{x}_h} \end{bmatrix}, \\ \bar{\boldsymbol{C}} &= \boldsymbol{\alpha}^T \boldsymbol{C} \alpha = \begin{bmatrix} \bar{\boldsymbol{C}}_{\boldsymbol{x}_r} & \bar{\boldsymbol{C}}_{\boldsymbol{x}_r,\boldsymbol{x}_h} \\ \bar{\boldsymbol{C}}_{\boldsymbol{x}_r,\boldsymbol{x}_h}^T & \bar{\boldsymbol{C}}_{\boldsymbol{x}_h} \end{bmatrix}, \\ \bar{\boldsymbol{K}} &= \boldsymbol{\alpha}^T \boldsymbol{K} \alpha = \begin{bmatrix} \bar{\boldsymbol{K}}_{\boldsymbol{x}_r} & \bar{\boldsymbol{K}}_{\boldsymbol{x}_r,\boldsymbol{x}_h} \\ \bar{\boldsymbol{K}}_{\boldsymbol{x}_r,\boldsymbol{x}_h}^T & \bar{\boldsymbol{K}}_{\boldsymbol{x}_h} \end{bmatrix}, \\ \bar{\boldsymbol{F}} &= \boldsymbol{\alpha}^T \boldsymbol{F} \end{aligned} \tag{A4}$$

The structure of these system matrices is shown in Fig. A1, where $\bar{\boldsymbol{M}}_{\boldsymbol{x}_r}$ represents the nonlinear component (relative DOFs) in the sector with a crack, $\bar{\boldsymbol{M}}_{\boldsymbol{x}_r,\boldsymbol{x}_{h,1}}$ represents the coupling between the nonlinear component and pristine component in the sector with a crack, and $\bar{\boldsymbol{M}}_{\boldsymbol{x}_{h,i}}$ represents the pristine component of the ith sector. The 1st sector is chosen as the sector with a crack in this work. Note that the pristine components $\bar{\boldsymbol{M}}_{\boldsymbol{x}_h}$, $\bar{\boldsymbol{C}}_{\boldsymbol{x}_h}$, and $\bar{\boldsymbol{K}}_{\boldsymbol{x}_h}$ in these matrices are obtained using the α transformation. These components can be computed from single-sector calculations [36] using a cyclic symmetric analysis. Explicit expressions for the submatrices of $\bar{\boldsymbol{M}}$ can be described as ($\bar{\boldsymbol{C}}$ and $\bar{\boldsymbol{K}}$ have the same expressions)

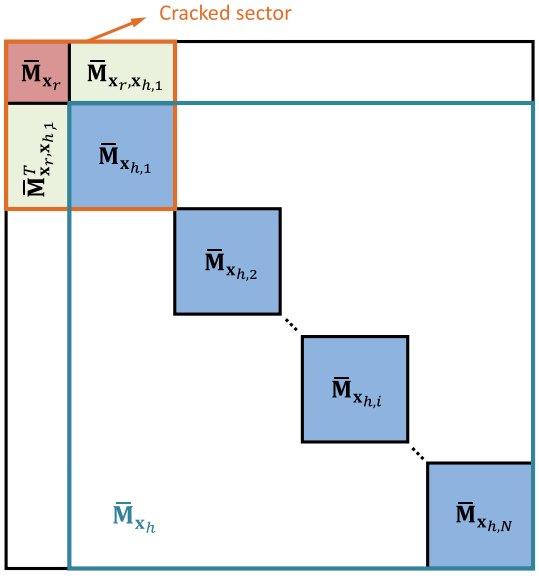

Fig. A1 Conceptual structure of $\bar{\boldsymbol{M}}$.

$$\begin{aligned} \bar{\boldsymbol{M}}_{\boldsymbol{x}_r} &= \boldsymbol{M}_{c1,c1}, \\ \bar{\boldsymbol{M}}_{\boldsymbol{x}_r,\boldsymbol{x}_h} &= [\boldsymbol{M}_{c1,c1} + \boldsymbol{M}_{c1,c2} \quad \boldsymbol{M}_{c1,l}], \\ \bar{\boldsymbol{M}}_{\boldsymbol{x}_h} &= \begin{bmatrix} \boldsymbol{M}_{c1,c1} + \boldsymbol{M}_{c1,c2}^T + \boldsymbol{M}_{c1,c2} + \boldsymbol{M}_{c2,c2} & \boldsymbol{M}_{c1,l} + \boldsymbol{M}_{c2,l} \\ \boldsymbol{M}_{c1,l}^T + \boldsymbol{M}_{c2,l}^T & \boldsymbol{M}_{l,l} \end{bmatrix} \end{aligned} \tag{A5}$$

Next, a modified CB-CMS method is used to reduce the model size by keeping the contacting DOFs grouped in $\boldsymbol{x}_r$ active while reducing all other DOFs grouped in $\boldsymbol{x}_h$ using a truncated set of normal modes. Furthermore, crack acceleration modes can also be employed in the reduction process to accelerate the convergence for the case when the crack is large. The modified Craig-Bampton transformation matrix $\boldsymbol{\beta}$ can be expressed as

$$\boldsymbol{\beta} = \begin{bmatrix} \boldsymbol{I} & \boldsymbol{\Phi}_{\mathrm{CB}_c}^r & \boldsymbol{0} \\ \boldsymbol{\Psi}_c & \boldsymbol{\Phi}_{\mathrm{CB}_c} & \boldsymbol{\Phi}_{n,1} \\ \boldsymbol{0} & \boldsymbol{0} & \boldsymbol{\Phi}_{n,2} \\ \vdots & \vdots & \vdots \\ \boldsymbol{0} & \boldsymbol{0} & \boldsymbol{\Phi}_{n,i} \\ \vdots & \vdots & \vdots \\ \boldsymbol{0} & \boldsymbol{0} & \boldsymbol{\Phi}_{n,N} \end{bmatrix} \tag{A6}$$

where $\boldsymbol{\Psi}_c$ represents the constraint modes, $\boldsymbol{\Phi}_{\mathrm{CB}_c}$ represents the crack acceleration modes with the relative displacement between contact pairs denoted by $\boldsymbol{\Phi}_{\mathrm{CB}_c}^r$, and $\boldsymbol{\Phi}_{n,i}$ are the normal modes of the ith sector. The computation of each mode is described as follows. The constraint modes $\boldsymbol{\Psi}_c$ are defined as the static displacement of the DOFs in $\boldsymbol{x}_h$ induced by successive unit displacement of each relative DOF grouped in $\boldsymbol{x}_r$, while all other relative DOFs are held fixed. Because these constraint modes are obtained by perturbing the DOFs along the crack surface, they can be treated as a localized deformation in the sector with a crack; thus, they can be approximated as zero in all other sectors and computed using only the sector with a crack. The crack acceleration modes $\boldsymbol{\Phi}_{\mathrm{CB}_c}$ represent the mode shapes of the sector with a crack that can be computed by solving the eigenvalue problem when its sector boundaries are fixed. Similarly, the normal modes $\boldsymbol{\Phi}_{n,i}$ can be computed by solving the eigenvalue problem for a healthy sector. Note that the pristine component of the full-bladed disk is cyclically symmetric; thus the model of a single sector is sufficient to construct the normal modes of the full system (i.e., $\boldsymbol{\Phi}_{n,i}$ for $i = 2, \ldots, N$ can be obtained by applying the appropriate phase

to $\boldsymbol{\Phi}_{n,1}$). The detailed description of cyclic expansion can be found in [36].

The size of $\boldsymbol{\beta}$ can be reduced dramatically by truncating the crack acceleration modes and the normal modes for the frequency range of interest. Reduced coordinates can then be obtained as

$$\bar{\boldsymbol{x}}_s = \boldsymbol{\beta}_s \boldsymbol{u}_s, \quad \bar{\boldsymbol{x}}_o = \boldsymbol{\beta}_o \boldsymbol{u}_o \tag{A7}$$

where $\bar{\boldsymbol{x}}_s$ and $\bar{\boldsymbol{x}}_o$ are the full coordinates of the system after applying the α transformation in its sliding state and open state, respectively; $\boldsymbol{u}_s$ and $\boldsymbol{u}_o$ are the reduced coordinates for the system after applying the $\boldsymbol{\beta}$ transformation in its sliding state and open state, respectively. In general, the full coordinates $\bar{\boldsymbol{x}}_s$ and $\bar{\boldsymbol{x}}_o$ share the same coordinate system if the gap between the contact surfaces is zero [29]; however, the reduced coordinates $\boldsymbol{u}_s$ and $\boldsymbol{u}_o$ are in different coordinate systems if the crack acceleration modes are used to construct $\boldsymbol{\beta}_s$ and $\boldsymbol{\beta}_o$. These crack acceleration modes are different in the sliding state and the open state. The equations of motion in the reduced space can then be obtained as

$$\begin{aligned}
&\boldsymbol{M}_{\mathrm{ROM},s}\ddot{\boldsymbol{u}}_s(t) + \boldsymbol{C}_{\mathrm{ROM},s}\dot{\boldsymbol{u}}_s(t) + \boldsymbol{K}_{\mathrm{ROM},s}\boldsymbol{u}_s(t) = \boldsymbol{F}_{\mathrm{ROM},s}(t),\\
&\boldsymbol{M}_{\mathrm{ROM},o}\ddot{\boldsymbol{u}}_o(t) + \boldsymbol{C}_{\mathrm{ROM},o}\dot{\boldsymbol{u}}_o(t) + \boldsymbol{K}_{\mathrm{ROM},o}\boldsymbol{u}_o(t) = \boldsymbol{F}_{\mathrm{ROM},o}(t)
\end{aligned} \tag{A8}$$

where

$$\begin{aligned}
\boldsymbol{M}_{\mathrm{ROM}} &= \boldsymbol{\beta}^T\bar{\boldsymbol{M}}\boldsymbol{\beta} = \begin{bmatrix} \boldsymbol{M}_{11} & \boldsymbol{M}_{12} & \boldsymbol{M}_{13} \\ \boldsymbol{M}_{12}^T & \boldsymbol{M}_{22} & \boldsymbol{M}_{23} \\ \boldsymbol{M}_{13}^T & \boldsymbol{M}_{23}^T & \boldsymbol{M}_{33} \end{bmatrix},\\
\boldsymbol{C}_{\mathrm{ROM}} &= \boldsymbol{\beta}^T\bar{\boldsymbol{C}}\boldsymbol{\beta} = \begin{bmatrix} \boldsymbol{C}_{11} & \boldsymbol{C}_{12} & \boldsymbol{C}_{13} \\ \boldsymbol{C}_{12}^T & \boldsymbol{C}_{22} & \boldsymbol{C}_{23} \\ \boldsymbol{C}_{13}^T & \boldsymbol{C}_{23}^T & \boldsymbol{C}_{33} \end{bmatrix},\\
\boldsymbol{K}_{\mathrm{ROM}} &= \boldsymbol{\beta}^T\bar{\boldsymbol{K}}\boldsymbol{\beta} = \begin{bmatrix} \boldsymbol{K}_{11} & \boldsymbol{K}_{12} & \boldsymbol{K}_{13} \\ \boldsymbol{K}_{12}^T & \boldsymbol{K}_{22} & \boldsymbol{K}_{23} \\ \boldsymbol{K}_{13}^T & \boldsymbol{K}_{23}^T & \boldsymbol{K}_{33} \end{bmatrix},\\
\boldsymbol{F}_{\mathrm{ROM}} &= \boldsymbol{\beta}^T\bar{\boldsymbol{F}}
\end{aligned} \tag{A9}$$

The submatrices of the $\boldsymbol{M}_{\mathrm{ROM}}$ can be expressed as ($\boldsymbol{C}_{\mathrm{ROM}}$ and $\boldsymbol{K}_{\mathrm{ROM}}$ have the same expressions in their submatrices)

$$\begin{aligned}
\boldsymbol{M}_{11} &= \bar{\boldsymbol{M}}_{\boldsymbol{x}_r} + \boldsymbol{\Psi}_c^T\bar{\boldsymbol{M}}^T_{\boldsymbol{x}_r,\boldsymbol{x}_{h,1}} + \bar{\boldsymbol{M}}_{\boldsymbol{x}_r,\boldsymbol{x}_{h,1}}\boldsymbol{\Psi}_c + \boldsymbol{\Psi}_c^T\bar{\boldsymbol{M}}_{\boldsymbol{x}_{h,1}}\boldsymbol{\Psi}_c,\\
\boldsymbol{M}_{12} &= \bar{\boldsymbol{M}}_{\boldsymbol{x}_r}\boldsymbol{\Phi}^r_{\mathrm{CB}_c} + \boldsymbol{\Psi}_c^T\bar{\boldsymbol{M}}^T_{\boldsymbol{x}_r,\boldsymbol{x}_{h,1}}\boldsymbol{\Phi}^r_{\mathrm{CB}_c} + \bar{\boldsymbol{M}}_{\boldsymbol{x}_r,\boldsymbol{x}_{h,1}}\boldsymbol{\Phi}_{\mathrm{CB}_c} + \boldsymbol{\Psi}_c^T\bar{\boldsymbol{M}}_{\boldsymbol{x}_{h,1}}\boldsymbol{\Phi}_{\mathrm{CB}_c},\\
\boldsymbol{M}_{13} &= \bar{\boldsymbol{M}}_{\boldsymbol{x}_r,\boldsymbol{x}_{h,1}}\boldsymbol{\Phi}_{n,1} + \boldsymbol{\Psi}_c^T\bar{\boldsymbol{M}}_{\boldsymbol{x}_{h,1}}\boldsymbol{\Phi}_{n,1},\\
\boldsymbol{M}_{22} &= \boldsymbol{\Phi}^{r^T}_{\mathrm{CB}_c}\bar{\boldsymbol{M}}_{\boldsymbol{x}_r}\boldsymbol{\Phi}^r_{\mathrm{CB}_c} + \boldsymbol{\Phi}^T_{\mathrm{CB}_c}\bar{\boldsymbol{M}}^T_{\boldsymbol{x}_r,\boldsymbol{x}_{h,1}}\boldsymbol{\Phi}^r_{\mathrm{CB}_c} + \boldsymbol{\Phi}^{r^T}_{\mathrm{CB}_c}\bar{\boldsymbol{M}}_{\boldsymbol{x}_r,\boldsymbol{x}_{h,1}}\boldsymbol{\Phi}_{\mathrm{CB}_c}\\
&\quad + \boldsymbol{\Phi}^T_{\mathrm{CB}_c}\bar{\boldsymbol{M}}_{\boldsymbol{x}_{h,1}}\boldsymbol{\Phi}_{\mathrm{CB}_c},\\
\boldsymbol{M}_{23} &= \boldsymbol{\Phi}^{r^T}_{\mathrm{CB}_c}\bar{\boldsymbol{M}}_{\boldsymbol{x}_r,\boldsymbol{x}_{h,1}}\boldsymbol{\Phi}_{n,1} + \boldsymbol{\Phi}^T_{\mathrm{CB}_c}\bar{\boldsymbol{M}}_{\boldsymbol{x}_{h,1}}\boldsymbol{\Phi}_{n,1},\\
\boldsymbol{M}_{33} &= \sum_{i=1}^{N}\boldsymbol{\Phi}^T_{n,i}\bar{\boldsymbol{M}}_{\boldsymbol{x}_{h,i}}\boldsymbol{\Phi}_{n,i}
\end{aligned} \tag{A10}$$

Note that $\boldsymbol{M}_{33} = \sum_{i=1}^{N}\boldsymbol{\Phi}^T_{n,i}\bar{\boldsymbol{M}}_{\boldsymbol{x}_{h,i}}\boldsymbol{\Phi}_{n,i} = \boldsymbol{I}$ and $\boldsymbol{K}_{33} = \sum_{i=1}^{N}\boldsymbol{\Phi}^T_{n,i}\bar{\boldsymbol{K}}_{\boldsymbol{x}_{h,i}}\boldsymbol{\Phi}_{n,i} = \boldsymbol{\Lambda}_0$, where $\boldsymbol{\Lambda}_0$ is the eigenvalue matrix of the corresponding pristine structure. All the submatrices in Eq. (A9) are computed using sector-level matrices and mode shapes; thus, the ROM of the full system can be constructed using single-sector models and calculations, which leads to significant computational savings.

Appendix B: BAA Method

This appendix discusses the response approximation process using the BAA method [29,32]. First, a secondary modal reduction is applied to the ROM of the mistuned system. The reduction is achieved by projecting the equations of motion along subsets of mode shapes that dominate the motion of the system in its sliding state and open state. These mode shapes can be obtained by computing the eigenvectors of ($\boldsymbol{K}^m_{\mathrm{ROM},s}$, $\boldsymbol{M}_{\mathrm{ROM},s}$) and ($\boldsymbol{K}^m_{\mathrm{ROM},o}$, $\boldsymbol{M}_{\mathrm{ROM},o}$), and are grouped in matrices $\boldsymbol{\Phi}^m_s$ and $\boldsymbol{\Phi}^m_o$, respectively. Equation (7) can then be projected along $\boldsymbol{\Phi}^m_s$ and $\boldsymbol{\Phi}^m_o$ using the modal transformations $\boldsymbol{u}_s = \boldsymbol{\Phi}^m_s\boldsymbol{q}_s$ and $\boldsymbol{u}_o = \boldsymbol{\Phi}^m_o\boldsymbol{q}_o$, where $\boldsymbol{q}_s$ and $\boldsymbol{q}_o$ are modal coordinates:

$$\begin{aligned}
&\boldsymbol{\Phi}^{mT}_s\boldsymbol{M}_{\mathrm{ROM},s}\boldsymbol{\Phi}^m_s\ddot{\boldsymbol{q}}_s + \boldsymbol{\Phi}^{mT}_s(\alpha\boldsymbol{M}_{\mathrm{ROM},s} + \beta\boldsymbol{K}^m_{\mathrm{ROM},s})\boldsymbol{\Phi}^m_s\dot{\boldsymbol{q}}_s\\
&\quad + \boldsymbol{\Phi}^{mT}_s\boldsymbol{K}^m_{\mathrm{ROM},s}\boldsymbol{\Phi}^m_s\boldsymbol{q}_s = \boldsymbol{\Phi}^{mT}_s\boldsymbol{F}_{\mathrm{ROM},s}(t),\\
&\boldsymbol{\Phi}^{mT}_o\boldsymbol{M}_{\mathrm{ROM},o}\boldsymbol{\Phi}^m_o\dot{\boldsymbol{q}}_o + \boldsymbol{\Phi}^{mT}_o(\alpha\boldsymbol{M}_{\mathrm{ROM},o} + \beta\boldsymbol{K}^m_{\mathrm{ROM},o})\boldsymbol{\Phi}^m_o\dot{\boldsymbol{q}}_o\\
&\quad + \boldsymbol{\Phi}^{mT}_o\boldsymbol{K}^m_{\mathrm{ROM},o}\boldsymbol{\Phi}^m_o\boldsymbol{q}_o = \boldsymbol{\Phi}^{mT}_o\boldsymbol{F}_{\mathrm{ROM},o}(t)
\end{aligned} \tag{B1}$$

Equation (B1) can also be expressed as a set of decoupled modal equations because they are proportionally damped

$$\begin{aligned}
&\ddot{q}_{s,j} + 2\zeta_{s,j}\omega_{s,j}\dot{q}_{s,j} + \omega^2_{s,j}q_{s,j} = f_{s,j}, \qquad j = 1, \ldots, N_s,\\
&\ddot{q}_{o,k} + 2\zeta_{o,k}\omega_{o,k}\dot{q}_{o,k} + \omega^2_{o,k}q_{o,k} = f_{o,k}, \qquad k = 1, \ldots, N_o
\end{aligned} \tag{B2}$$

where N_s and N_o are the numbers of mode shapes used to project the motion in the sliding and open state, respectively; ($\omega_{s,j}$, $\omega_{o,k}$) and ($\zeta_{s,j}$, $\zeta_{o,k}$) are the undamped natural frequencies and the viscous damping ratios associated with the jth mode in the sliding state and the kth mode in the open state, respectively; ($f_{s,j}$, $f_{o,k}$) are the modal forces. The modal forces can be expressed in the following form if the system is excited by harmonic forcing:

$$\begin{aligned}
f_{s,j}(t) &= f_{\mathrm{sc},j}\cos(\omega t) + f_{\mathrm{ss},j}\sin(\omega t),\\
f_{o,k}(t) &= f_{\mathrm{oc},k}\cos(\omega t) + f_{\mathrm{os},k}\sin(\omega t)
\end{aligned} \tag{B3}$$

The modal coordinates $q_{s,j}$ and $q_{o,k}$ can then be symbolically expressed as combinations of the linear transient response and the linear steady-state response:

$$\begin{aligned}
q_{s,j}(t) &= e^{-\zeta_{s,j}\omega_{s,j}t}[s_{1,j}\cos(\omega_{\mathrm{sd},j}t) + s_{2,i}\sin(\omega_{\mathrm{sd},j}t)]\\
&\quad + \frac{f_{\mathrm{sc},j}\cos(\omega t - \theta_{s,j} + \psi) + f_{\mathrm{ss},j}\sin(\omega t - \theta_{s,j} + \psi)}{\omega^2_{s,j}\sqrt{[1 - (\omega/\omega_{s,j})^2]^2 + (2\zeta_{s,j}\omega/\omega_{s,j})^2}},\\
q_{o,k}(t) &= e^{-\zeta_{o,k}\omega_{o,k}t}[o_{1,k}\cos(\omega_{\mathrm{od},k}t) + o_{2,j}\sin(\omega_{\mathrm{od},k}t)]\\
&\quad + \frac{f_{\mathrm{oc},k}\cos(\omega t - \theta_{o,k} + \psi) + f_{\mathrm{os},k}\sin(\omega t - \theta_{o,k} + \psi)}{\omega^2_{o,k}\sqrt{[1 - (\omega/\omega_{o,k})^2]^2 + (2\zeta_{o,k}\omega/\omega_{o,k})^2}}
\end{aligned} \tag{B4}$$

where $\omega_{\mathrm{sd},j}$ and $\omega_{\mathrm{od},k}$ are the damped frequencies; $\theta_{s,j} = \tan^{-1}(2\zeta_{s,j}\omega_{s,j}\omega/\omega^2_{s,j} - \omega^2)$, and $\theta_{o,k} = \tan^{-1}(2\zeta_{o,k}\omega_{o,k}\omega/\omega^2{}_{o,k} - \omega^2)$; $s_{1,j}$, $s_{2,j}$, $o_{1,k}$, and $o_{2,k}$ are scalar coefficients of the linear transient responses; ψ represents an additional phase angle between the external force and the linear steady-state responses caused by the nonlinearity.

Next, the motion of an entire nonlinear vibration cycle is approximated by coupling the linear response in the sliding state and the linear response in the open state. The state of the system is determined by the state of the relative DOFs shown in Fig. B1a. The system is in the sliding state when $\tilde{\boldsymbol{x}}_r \le \boldsymbol{0}$ and is in the open state when $\tilde{\boldsymbol{x}}_r > \boldsymbol{0}$, where $\tilde{\boldsymbol{x}}_r$ represents the relative DOFs in the contact direction ($\tilde{\boldsymbol{x}}_r$ is a subset of $\boldsymbol{x}_r$). Note that the amount of penetration between the contacting nodes ($|\tilde{x}_{r,i}|$) in the sliding state is reduced when a higher contacting stiffness value k^* is used. T_s is the time that the system

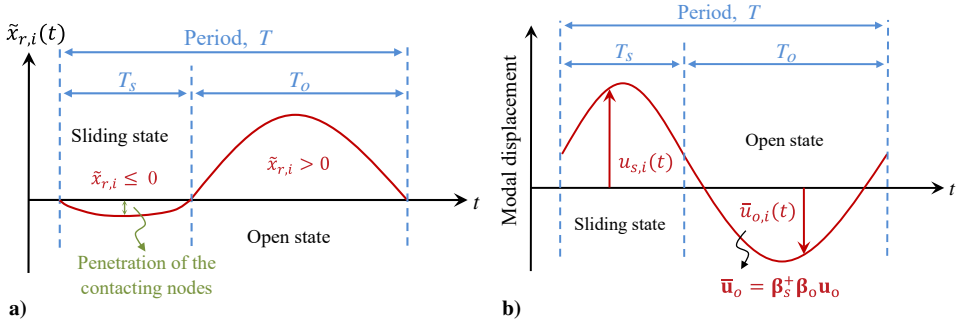

Fig. B1 a) Schematic plot of a steady-state vibration cycle. b) The relationship between the two modal coordinate systems.

spends in the sliding state and T_o represents the time that the system spends in the open state. Furthermore, as mentioned in Appendix A, the reduced coordinates $\boldsymbol{u}_s$ and $\boldsymbol{u}_o$ represent different coordinate systems. To couple the linear responses in the two linear states, an appropriate transformation is needed. Thus, the reduced space of the open system is projected onto the reduced space of the sliding system using $\bar{\boldsymbol{u}}_o = \boldsymbol{\beta}_s^+ \boldsymbol{\beta}_o \boldsymbol{u}_o$, where $\boldsymbol{\beta}_s^+$ is the pseudo-inverse of $\boldsymbol{\beta}_s$. The motion for all DOFs in this reduced space is schematically shown in Fig. B1b. The compatibility conditions for the displacement and velocity are then applied at the moment when the system switches from one state to the other. These compatibility conditions are directly applied to the reduced coordinates and are summarized as follows:

$$\begin{aligned}
\tilde{\boldsymbol{x}}_{o,r}(T_s) &= \mathbf{0},\\
\tilde{\boldsymbol{x}}_{o,r}(T_s + T_o) &= \mathbf{0},\\
\boldsymbol{u}_s(T_s) &= \bar{\boldsymbol{u}}_o(T_s),\\
\boldsymbol{u}_s(0) &= \bar{\boldsymbol{u}}_o(T_s + T_o),\\
\dot{\hat{\boldsymbol{u}}}_s(T_s) &= \dot{\hat{\boldsymbol{u}}}_o(T_s),\\
\dot{\hat{\boldsymbol{u}}}_s(0) &= \dot{\hat{\boldsymbol{u}}}_o(T_s + T_o)
\end{aligned} \tag{B5}$$

where $\dot{\hat{\boldsymbol{u}}}_s$ and $\dot{\hat{\boldsymbol{u}}}_o$ are the components of the velocity in the overlapping space of $\boldsymbol{\Phi}_s^m$ and $\boldsymbol{\Phi}_o^m$. The BAA method assumes that the continuity of the velocity of the system is only satisfied in the overlapping space because $\boldsymbol{\Phi}_s^m$ and $\boldsymbol{\Phi}_o^m$ do not occupy the same vector space. This overlapping space is obtained from the following: 1) $\boldsymbol{\beta}_s \boldsymbol{\Phi}_s^m$ and $\boldsymbol{\beta}_o \boldsymbol{\Phi}_o^m$ are grouped into a single matrix; 2) the left-singular vectors associated with the largest singular values of the matrix are selected as the basis of the full overlapping space $\boldsymbol{\Phi}_{\text{Full}}$; 3) the full overlapping space is projected onto the reduced space using $\boldsymbol{\Phi} = \boldsymbol{\beta}_s^+ \boldsymbol{\Phi}_{\text{Full}}$. The velocity components of the overlapping space are computed from $\dot{\hat{\boldsymbol{u}}}_s = \boldsymbol{T}_v \dot{\boldsymbol{u}}_s$ and $\dot{\hat{\boldsymbol{u}}}_o = \boldsymbol{T}_v \dot{\boldsymbol{u}}_o$, where $\boldsymbol{T}_v$ is the projection matrix defined as $\boldsymbol{T}_v = \boldsymbol{\Phi}(\boldsymbol{\Phi}^T \boldsymbol{\Phi})^{-1} \boldsymbol{\Phi}^T$. Equation (B5) can be expressed in terms of modal coordinates as

$$\begin{aligned}
\tilde{\boldsymbol{\beta}}_{o,r} \boldsymbol{\Phi}_o^m \boldsymbol{q}_o(T_s) &= \mathbf{0},\\
\tilde{\boldsymbol{\beta}}_{o,r} \boldsymbol{\Phi}_o^m \boldsymbol{q}_o(T_s + T_o) &= \mathbf{0},\\
\boldsymbol{\Phi}^T \boldsymbol{\Phi}_s^m \boldsymbol{q}_s(T_s) &= \boldsymbol{\Phi}^T \bar{\boldsymbol{\Phi}}_o^m \boldsymbol{q}_o(T_s),\\
\boldsymbol{\Phi}^T \boldsymbol{\Phi}_s^m \boldsymbol{q}_s(0) &= \boldsymbol{\Phi}^T \bar{\boldsymbol{\Phi}}_o^m \boldsymbol{q}_o(T_s + T_o),\\
\boldsymbol{\Phi}^T \hat{\boldsymbol{\Phi}}_s^m \dot{\boldsymbol{q}}_s(T_s) &= \boldsymbol{\Phi}^T \hat{\boldsymbol{\Phi}}_o^m \dot{\boldsymbol{q}}_o(T_s),\\
\boldsymbol{\Phi}^T \hat{\boldsymbol{\Phi}}_s^m \dot{\boldsymbol{q}}_s(0) &= \boldsymbol{\Phi}^T \hat{\boldsymbol{\Phi}}_o^m \dot{\boldsymbol{q}}_o(T_s + T_o)
\end{aligned} \tag{B6}$$

where $\tilde{\boldsymbol{\beta}}_{o,r}$ is the portion of $\boldsymbol{\beta}_o$ with the relative DOFs in the contact direction; $\bar{\boldsymbol{\Phi}}_o^m = \boldsymbol{\beta}_s^+ \boldsymbol{\beta}_o \boldsymbol{\Phi}_o^m$ is the transformed mode shapes of the system in its open state; $\hat{\boldsymbol{\Phi}}_s^m$ and $\hat{\boldsymbol{\Phi}}_o^m$ can be computed using $\hat{\boldsymbol{\Phi}}_s^m = \boldsymbol{T}_v \boldsymbol{\Phi}_s^m$, and $\hat{\boldsymbol{\Phi}}_o^m = \boldsymbol{T}_v \bar{\boldsymbol{\Phi}}_o^m$. Note that $T_s + T_o$ is the period of a steady-state nonlinear vibration cycle that can be calculated by $T_s + T_o = 2\pi/\omega$ and T_s is an unknown in Eq. (B6). The total number of scalar equations from Eq. (B5) can be quite large for a complex system. Thus, these equations are premultiplied by $\boldsymbol{\Phi}^T$ to reduce the required computational cost.

Next, a nonlinear optimization solver (e.g., the function "lsqnonlin" in MATLAB) can be used to solve for the unknowns ($s_{1,i}$, $s_{2,i}$, $o_{1,j}$, $o_{2,j}$, ψ, and T_s) in Eq. (B6) by minimizing its residual. Then, the physical displacements $\boldsymbol{x}_s$ and $\boldsymbol{x}_o$ are expanded from the modal coordinates using $\boldsymbol{x}_s = \alpha \boldsymbol{\beta}_s \boldsymbol{\Phi}_s^m \boldsymbol{q}_s$ and $\boldsymbol{x}_o = \alpha \boldsymbol{\beta}_o \boldsymbol{\Phi}_o^m \boldsymbol{q}_o$. The nonlinear vibration cycle is then constructed using $\boldsymbol{x}_s$, $\boldsymbol{x}_o$, and the transition time T_s. Finally, an efficient frequency sweep can be carried out to estimate the forced response for a bladed disk with a crack. Note that Eq. (B6) might possess multiple solutions; thus, an appropriate selection of initial values for the unknowns at the starting frequency point is needed to obtain a physically valid solution [29].

Acknowledgments

This paper is based on work partially supported by the National Science Foundation under Grant No. 1902408, program manager Robert Landers. Any opinions, findings, and conclusions or recommendations expressed in this paper are those of the authors and do not necessarily reflect the views of the National Science Foundation. The authors would also like to acknowledge the financial support from the Future Academic Scholars Training program of the Department of Mechanical and Aerospace Engineering at The Ohio State University.

References

[1] Lim, S.-H., Bladh, R., Castanier, M. P., and Pierre, C., "Compact, Generalized Component Mode Mistuning Representation for Modeling Bladed Disk Vibration," *AIAA Journal*, Vol. 45, No. 9, 2007, pp. 2285–2298. doi:10.2514/1.13172

[2] Dye, R. C. F., and Henry, T. A., "Vibration Amplitudes of Compressor Blades Resulting from Scatter in Blade Natural Frequencies," *ASME Journal of Engineering for Power*, Vol. 91, No. 3, 1969, pp. 182–188. doi:10.1115/1.3574726

[3] Ewins, D. J., "The Effects of Detuning Upon the Forced Vibrations of Bladed Disks," *Journal of Sound and Vibration*, Vol. 9, No. 1, 1969, pp. 65–79. doi:10.1016/0022-460X(69)90264-8

[4] Griffin, J. H., and Hoosac, T. M., "Model Development and Statistical Investigation of Turbine Blade Mistuning," *ASME Journal of Vibration, Acoustics, Stress, and Reliability in Design*, Vol. 106, No. 2, 1984, pp. 204–210. doi:10.1115/1.3269170

[5] Wei, S.-T., and Pierre, C., "Localization Phenomena in Mistuned Assemblies with Cyclic Symmetry Part I: Free Vibrations," *ASME Journal of Vibration, Acoustics, Stress, and Reliability in Design*, Vol. 110, No. 4, 1988, pp. 429–438. doi:10.1115/1.3269547

[6] Wei, S.-T., and Pierre, C., "Localization Phenomena in Mistuned Assemblies with Cyclic Symmetry Part II: Forced Vibrations," *ASME Journal of Vibration, Acoustics, Stress, and Reliability in Design*, Vol. 110, No. 4, 1988, pp. 439–449. doi:10.1115/1.3269548

[7] Yang, M.-T., and Griffin, J. H., "A Reduced-Order Model of Mistuning Using a Subset of Nominal System Modes," *Journal of Engineering for Gas Turbines and Power—Transactions of the ASME*, Vol. 123, No. 4,

1999, pp. 893–900.
doi:10.1115/1.1385197
[8] Feiner, D. M., and Griffin, J. H., "A Fundamental Model of Mistuning for a Single Family of Modes," *Journal of Turbomachinery*, Vol. 124, No. 4, 2002, pp. 597–605.
doi:10.1115/1.1508384
[9] Gan, Y., Mayer, J. L., D'Souza, K. X., and Epureanu, B. I., "A Mode-Accelerated XXr (MAX) Method for Complex Structures with Large Blends," *Mechanical Systems and Signal Processing*, Vol. 93, Sept. 2017, pp. 1–15.
doi:10.1016/j.ymssp.2017.01.042
[10] Kurstak, E., and D'Souza, K., "Multistage Blisk and Large Mistuning Modeling Using Fourier Constraint Modes and PRIME," *Journal of Engineering for Gas Turbines and Power—Transactions of the ASME*, Vol. 140, No. 7, 2018, Paper 072505.
doi:10.1115/1.4038613
[11] Kurstak, E., Wilber, R., and D'Souza, K., "Parametric Reduced Order Models for Bladed Disks with Mistuning and Varying Operational Speed," *Journal of Engineering for Gas Turbines and Power*, Vol. 141, No. 5, 2019, Paper 051018.
doi:10.1115/1.4041204
[12] Guyan, R. J., "Reduction of Stiffness and Mass Matrices," *AIAA Journal*, Vol. 3, No. 2, 1965, p. 380.
doi:10.2514/3.2874
[13] Friswell, M. I., Penny, J. E. T., and Garvey, S. D., "Using Linear Model Reduction to Investigate the Dynamics of Structures with Local Non-Linearities," *Mechanical Systems and Signal Processing*, Vol. 9, No. 3, 1995, pp. 317–328.
doi:10.1006/mssp.1995.0026
[14] O'Callahan, J., Avitabile, P., and Riemer, R., "System Equivalent Reduction Expansion Process (SEREP)," *Proceedings of the 7th International Modal Analysis Conference*, Union College, Schenectady, NY, 1989, pp. 29–37.
[15] Bennighof, J. K., and Lehoucq, R. B., "An Automated Multilevel Substructuring Method for Eigenspace Computation in Linear Elastodynamics," *SIAM Journal on Scientific Computing*, Vol. 25, No. 6, 2004, pp. 2084–2106.
doi:10.1137/S1064827502400650
[16] Theodosiou, C., and Natsiavas, S., "Dynamics of Finite Element Structural Models with Multiple Unilateral Constraints," *International Journal of Non-Linear Mechanics*, Vol. 44, No. 4, 2009, pp. 371–382.
doi:10.1016/j.ijnonlinmec.2009.01.006
[17] Craig, R. R., and Bampton, M. C. C., "Coupling of Substructures for Dynamic Analyses," *AIAA Journal*, Vol. 6, No. 7, 1968, pp. 1313–1319.
doi:10.2514/3.4741
[18] Krattiger, D., Wu, L., Zacharczuk, M., Buck, M., Kuether, R. J., Allen, M. S., Tiso, P., and Brake, M. R., "Interface Reduction for Hurty/Craig-Bampton Substructured Models: Review and Improvements," *Mechanical Systems and Signal Processing*, Vol. 114, Jan. 2019, pp. 579–603.
doi:10.1016/j.ymssp.2018.05.031
[19] Marinescu, O., Epureanu, B., and Banu, M., "Reduced Order Models of Mistuned Cracked Bladed Disks," *Journal of Vibration and Acoustics*, Vol. 133, No. 5, 2011, Paper 051014.
doi:10.1115/1.4003940
[20] Blair, K. B., Krousgrill, C. M., and Farris, T. N., "Harmonic Balance and Continuation Techniques in the Dynamic Analysis of Duffing's Equation," *Journal of Sound and Vibration*, Vol. 202, No. 5, 1997, pp. 717–731.
doi:10.1006/jsvi.1996.0863
[21] Cigeroglu, E., An, N., and Menq, C.-H., "A Microslip Friction Model with Normal Load Variation Induced by Normal Motion," *Nonlinear Dynamics*, Vol. 50, No. 3, 2007, pp. 609–626.
doi:10.1007/s11071-006-9171-4
[22] Saito, A., Castanier, M. P., Pierre, C., and Poudou, O., "Efficient Nonlinear Vibration Analysis of the Forced Response of Rotating Cracked Blades," *Journal of Computational and Nonlinear Dynamics—Transactions of the ASME*, Vol. 4, No. 1, 2009, Paper 011005.
doi:10.1115/1.3007908
[23] Firrone, C. M., Zucca, S., and Gola, M. M., "The Effect of Underplatform Dampers on the Forced Response of Bladed Disks by a Coupled Static/Dynamic Harmonic Balance Method," *International Journal of Non-Linear Mechanics*, Vol. 46, No. 2, 2011, pp. 363–375.
doi:10.1016/j.ijnonlinmec.2010.10.001
[24] Jung, C., Saito, A., and Epureanu, B. I., "Detection of Cracks in Mistuned Bladed Disks Using Reduced-Order Models and Vibration Data," *Journal of Vibration and Acoustics—Transactions of the ASME*, Vol. 134, No. 6, 2012, Paper 061010.
doi:10.1115/1.4007244
[25] Zucca, S., and Epureanu, B. I., "Reduced Order Models for Nonlinear Dynamic Analysis of Structures with Intermittent Contacts," *Journal of Vibration and Control*, Vol. 24, No. 12, 2018, pp. 2591–2604.
doi:10.1177/1077546316689214
[26] Zucca, S., "On the Dual Craig–Bampton Method for the Forced Response of Structures with Contact Interfaces," *Nonlinear Dynamics*, Vol. 87, No. 4, 2017, pp. 2445–2455.
doi:10.1007/s11071-016-3202-6
[27] Shampine, L. F., and Reichelt, M. W., "The MATLAB ODE Suite," *SIAM Journal on Scientific Computing*, Vol. 18, No. 1, 1997, pp. 1–22.
doi:10.1137/S1064827594276424
[28] Jung, C., D'Souza, K., and Epureanu, B. I., "Nonlinear Amplitude Approximation for Bilinear Systems," *Journal of Sound and Vibration*, Vol. 333, No. 13, 2014, pp. 2909–2919.
doi:10.1016/j.jsv.2014.01.029
[29] Tien, M.-H., and D'Souza, K., "A Generalized Bilinear Amplitude and Frequency Approximation for Piecewise-Linear Nonlinear Systems with Gaps or Prestress," *Nonlinear Dynamics*, Vol. 88, No. 4, 2017, pp. 2403–2416.
doi:10.1007/s11071-017-3385-5
[30] Tien, M.-H., and D'Souza, K., "Analyzing Bilinear Systems Using a New Hybrid Symbolic-Numeric Computational Method," *Journal of Vibration and Acoustics*, Vol. 141, No. 3, 2019, Paper 031008.
doi:10.1115/1.4042520
[31] Tien, M.-H., and D'Souza, K., "Transient Dynamics Analysis of Cracked Structures with Multiple Contact Pairs Using Generalized HSNC," *Nonlinear Dynamics*, Vol. 96, No. 2, 2019, pp. 1115–1131.
doi:10.1007/s11071-019-04844-7
[32] Tien, M.-H., Hu, T., and D'Souza, K., "Generalized Bilinear Amplitude Approximation and X-Xr for Modeling Cyclically Symmetric Structures with Cracks," *Journal of Vibration and Acoustics*, Vol. 140, No. 4, 2018, Paper 041012.
doi:10.1115/1.4039296
[33] Castanier, M. P., and Pierre, C., "Modeling and Analysis of Mistuned Bladed Disk Vibration: Status and Emerging Directions," *Journal of Propulsion and Power*, Vol. 22, No. 2, 2006, pp. 384–396.
doi:10.2514/1.16345
[34] Newmark, N. M., "A Method of Computation for Structural Dynamics," *Journal of Engineering Mechanics*, Vol. 85, No. 3, 1959, pp. 67–94.
[35] Bladh, R., Pierre, C., Castanier, M. P., and Kruse, M. J., "Dynamic Response Predictions for a Mistuned Industrial Turbomachinery Rotor Using Reduced-Order Modeling," *Journal of Engineering for Gas Turbines and Power*, Vol. 124, No. 2, 2002, pp. 311–324.
doi:10.1115/1.1447236
[36] Olson, B. J., Shaw, S. W., Shi, C., Pierre, C., and Parker, R. G., "Circulant Matrices and Their Application to Vibration Analysis," *ASME Applied Mechanics Reviews*, Vol. 66, No. 4, 2014, Paper 040803.
doi:10.1115/1.4027722

R Ohayon
Associate Editor